

Super-Convergent Meshless Computations for Active Vibration Control of Bi-Directional Functionally Graded Terfenol-D Beams with Twisted Geometry

Mukund A. Patil, Tanmoy Mukhopadhyay, and Susmita Naskar*

This paper presents a superconvergent meshless numerical approach based on generalized differential quadrature method to analyze the dynamic behavior of bidirectional functionally graded aluminum-Terfenol-D beams with twisted geometry. The power-law exponent model is exploited to modify the material properties, such as Young's modulus and mass density, over the whole thickness and longitudinal direction of the bidirectional functionally graded aluminum-Terfenol-D beams. The influences of Terfenol-D's bidirectional gradation, porosity volume fraction index, twisted angle, and viscoelastic boundary conditions are investigated on the dynamic characteristics with the notion of developing a design-oriented mapping of the input parameter space. Subsequently, the study delves into the effectiveness of Terfenol-D in vibration control for complex twisted structural systems. Computational investigations are conducted to demonstrate the impact of gain control, and the characteristics and optimal arrangement of Terfenol-D patches on the dynamic response of active sandwich beams under transverse impulsive loads. The findings show that the implementation of active vibration control exploiting Terfenol-D's magnetostrictive qualities can have a significant impact on reducing the oscillations of bidirectional functionally graded beams. The control studies reveal that placing five Terfenol-D patches at $L/5$ provides the most effective damping, compared to placement at $L/3$ or using a full Terfenol-D layer. The findings highlight the potential of strategically graded and patch-configured magnetostrictive layers for tailoring vibration behavior in complex structural systems.

1. Introduction

Throughout the last few decades, dynamics, and free vibration analysis of twisted beams have piqued researchers' curiosity. Pre-twisted beams are one of the most crucial structural components and are widely employed in several contemporary industrial sectors, including nuclear, automotive, aerospace and renewable energy. One of the main causes of vibration is the dynamic forces imparted by the spinning cantilever beams. These structures must be operated safely and effectively, which requires vibration analysis and suppression. In recent years, there have seen a lot of studies on Terfenol-D and piezoelectric materials for vibration suppression. We provide a concise review concerning dynamics and vibration control exploiting such smart materials in the following paragraphs.

The aspect of vibration reduction using macrofiber composite actuators and sensors was investigated with the use of piezoelectric materials.^[1-4] A significant volume of research can be traced in the area of smart magneto-electro-active control of vibration in composite and laminated structures.^[5-12] Electro and magneto-active Smart materials and structures have been widely used in basic structural forms like

beams, plates and shells along with their derivative compound structures like metamaterials for active control, modulation and sensing.^[13-19] A significant amount of research can be found in literature concerning dynamic analysis of composites and functionally graded structures including their optimization, sensitivity analysis and uncertainty quantification.^[20-32] While thickness-wise functional gradation is traditionally investigated in the literature, length-wise and bi-directional gradation has received significant attention lately.^[33-37] In a thermal environment, the effects of hub radius, rotating speed, material properties, geometric imperfections, and elastic root rigidity on the natural frequencies, critical buckling loads, and instability regions of rotating pre-twisted functionally graded carbon nanotube reinforced composite imperfect beams were analyzed by Lin et al.^[38] On a rotating variable-thickness pre-twisted blade with elastic restrictions, a complete parametric evaluation of the impacts of thickness-taper ratio, pre-twist angle, rotational speed, and con-

M. A. Patil

Department of Mechanical Engineering

G. H. Raisoni College of Engineering & Management
Jalgaon, Maharashtra 425001, India

T. Mukhopadhyay, S. Naskar

School of Engineering

University of Southampton

Southampton SO17 1BJ, UK

E-mail: S.Naskar@soton.ac.uk

 The ORCID identification number(s) for the author(s) of this article can be found under <https://doi.org/10.1002/adts.202501394>

© 2025 The Author(s). Advanced Theory and Simulations published by Wiley-VCH GmbH. This is an open access article under the terms of the [Creative Commons Attribution](https://creativecommons.org/licenses/by/4.0/) License, which permits use, distribution and reproduction in any medium, provided the original work is properly cited.

DOI: [10.1002/adts.202501394](https://doi.org/10.1002/adts.202501394)

nection stiffness on blade modal properties was carried out by Li and Cheng.^[39] Rotational uncertainty of composite shells was quantified by Dey et al. based on a machine learning assisted finite element approach.^[40] On the free vibration characteristics of the rotating blade-shaft assembly, the effects of rotating speed, GPL distribution pattern, GPL weight fraction, length-to-thickness ratio, length-to-width ratio of GPLs, inner and outer radius of the disc, and pre-twist angle per unit length, setting angle, and length of the blade have been discussed by Zhao et al.^[41] They have talked about how slight changes in the pre-twist angle and blade setting angle lead to larger first travelling wave frequencies and lower third travelling wave frequencies. The coupled vibration model of a rotating FGGLRC pretwisted blade-shaft assembly was reported by Zhao et al.,^[42] where the spinning shaft and blade are modelled using the Euler-Bernoulli beam theory and Rayleigh beam theory, respectively. Comprehensive research has been reported by Cheng et al.^[43] on the effects of CNT arrangement, pre-twist angle, rotation speed, and stagger angle on the blade vibration. It has been discovered that adding carbon nanotubes significantly affects raising blade frequency. The large-amplitude vibrational behavior of rotating pre-twisted multilayer GPLRC blades in a thermal environment was studied by Guo et al.^[44] using a thermo-elastic dynamic model based on the first-order shear deformation theory and an improved version of the Novozhilov nonlinear shell theory. The stiffening/softening impact was modelled using nonlinear variables in the static analysis by Lotfan and Bediz.^[45] In light of this, it is becoming abundantly evident that there is a strong alternative to the finite element approach and the dynamic stiffness method, in which the derivative terms from the governing differential equation in the strong form are approximated on each grid point. The differential quadrature method uses weighting coefficients to estimate any-order derivatives at each grid point.^[46–48] The approach outperforms the standard finite element method, especially when higher precision of findings is required with minimal computational cost. In this paper, we would focus on developing a superconvergent meshless approach for the dynamic analysis of functionally graded Terfenol-D beams.

In order to solve the problem of free vibration in pre-twisted, functionally graded carbon nanotube-reinforced composite beams in a thermal environment, Chebyshev polynomials and the Ritz technique have been used as potential solutions.^[49] The free vibration of pretwisted beams was analyzed by Adair and Jaeger^[50] using an eigenvalue formulation based on the adomian modified decomposition method under clamped-free boundary conditions and rotating speeds. Wang and Yuan^[51] used 3D subparametric quadrature element approach to study beams with rectangular, circular, elliptical, and airfoil cross-sections, variable curvature and pre-twist rates, and various boundary conditions. The approach maps the irregular solid into a regular cube, extending the already-existing quadrature element method with regular forms. The free vibration of a rotating, pre-twisted beam with bending-bending-torsion coupling that is axially loaded by a tendon was studied by Ondra and Titurus.^[52] Free vibration, buckling, and dynamic stability of rotating pre-twisted functionally graded carbon nanotube reinforced composite imperfect beams in thermal environment was investigated by Lin et al.^[38] The Euler, Coriolis, and centrifugal force fields are primarily responsible for the different vibrational properties of spinning

structures compared to stationary ones, as it will be evident in the following paragraph.

Considering the prospective application cases for the dynamic analysis of twisted smart beams under consideration in this study, we further provide a brief literature review on such structures under rotating and aerodynamic conditions. A spinning pre-twisted beam with bending-bending torsion coupling axially loaded by a guided tendon so that the rotorcraft can function under a variety of operating situations was investigated by Wu and Titurus.^[53] With the help of the general Galerkin approach, the parametric instability of a pre-twisted beam with a top spring attachment and viscoelastic springs serving as end supports was examined by Nayak et al.^[54] The finite element technique was used to provide a numerical solution for analyzing the free vibrations of a spinning pre-twisted cylindrical shell made of composite materials reinforced with graphene.^[55] An investigation was conducted on a theoretical model that simulates the thermoelastic vibration analysis of functionally graded thermal barrier coated (FGTBC) blades.^[56] This model takes into account the non-uniformity of FGTBC materials, as well as rotational motions, including the Coriolis effect, prestress stiffening, and rotational softening. A study^[57] was conducted to simulate and analyze the behavior of a pre-twisted blade with tenon joints and under-platform dampers in a thermal environment and subjected to nonlinear loads. A novel model^[58] was introduced to analyze the vibrations and bifurcations of a pretwisted composite rotating blade that is strengthened by functionally graded graphene platelets (FGGP). This model considered the effects of the leakage flow at the tip clearance, aerodynamic force, and high rotating speed. The dynamic model of axial excitation produced by the aerodynamic force in the tip clearance, which includes two trigonometric functions with different frequencies, was investigated for functionally graded graphene platelet (FGGP)-reinforced rotating pretwisted composite blades under blade-casing rubbing and aerodynamic force.^[59] The first-order shear deformation theory was used to create a pre-twisted blade model based on Ti-SiC fiber reinforced composite and NACA four-digit airfoil utilizing Rayleigh-Ritz technique.^[60] The free vibration behavior of pre-twisted tapered rotating microbeams^[61] composed of bidirectional functionally graded material (BFGM) was studied using an improved mathematical model, wherein the first-order shear deformation theory was used to build the mathematical formulation in a global non-inertial frame with suitable transformations between the global and local frames. Shada et al.^[62] examined smart damping on bi-directionally tapered functionally graded sandwich plates. Kuriakose and Sreehari^[63] examined how temperature conditions affect the passive control of vibration and flutter in damaged composite plates with piezoelectric patches.

A careful review of the literature reveals that recent studies have explored the vibration characteristics and control of functionally graded beams, curved beams, fluid conveying pipes, incorporating magnetostrictive materials like Terfenol-D with different parametric studies such as free and forced vibration, partial foundation and different boundary conditions.^[46,64–69] Researchers have further examined^[70] the linear and non-linear vibration of Terfenol-D FGM beams with porosities, employing advanced numerical and semi-analytical methods. It is found that Terfenol-D outperforms in damping performance. While exist-

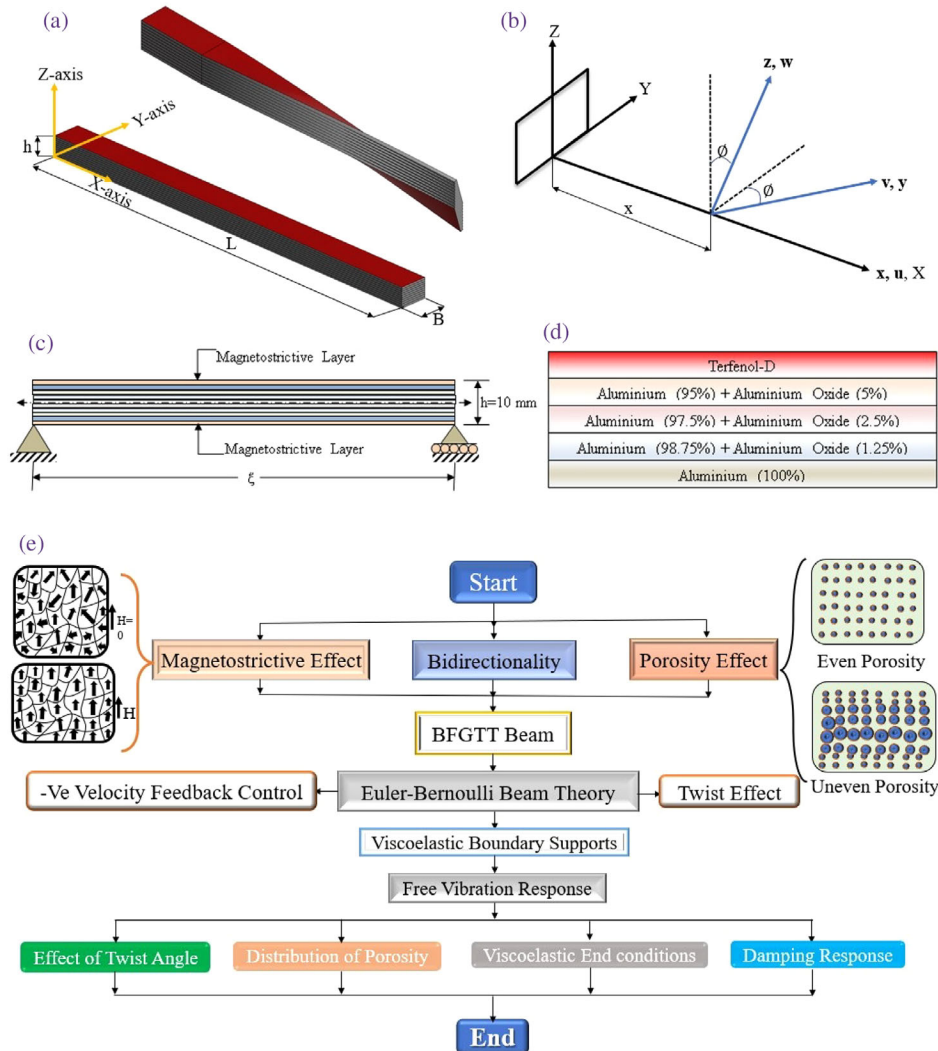


Figure 1. Dynamics of bidirectional functionally graded aluminum-Terfenol-D twisted beams. A) Schematic illustration of bidirectional functionally graded aluminium-Terfenol-D twisted beam. B) Rotation of point at a distance of x from the origin of BFG Al-Terfenol-D twisted beam. C) Schematics of layerwise structure of aluminum-Terfenol-D beam. D) Layerwise volume distribution of aluminum–aluminum oxide distribution. E) Detailed flowchart for dynamic analysis of bidirectional functionally graded aluminium-Terfenol-D twisted beams.

ing literature provides insights into the free vibration of twisted beams, research on vibration control of twisted beams incorporating smart actuators like Terfenol-D, coupled with the effects of material gradation and porosity, is scarce to find in literature. Moreover, the impact of non-classical boundary conditions, highly relevant in practical applications, has not been adequately explored in the context of twisted beam geometries. Thus, a significant gap exists in the understanding of free vibration and control of functionally graded twisted beams integrated with smart actuators, considering the combined influence of material gradation, porosity, and non-classical boundary conditions.

As a consequence, we aim to investigate the dynamics and active control of twisted smart beams with bi-directional Terfenol-D gradation (refer to **Figure 1A–D** in this paper. As an integral part of this study, the influence of manufacturing and geometric irregularities such as porosity^[71,72] will be examined on the dynamic behavior. In this context, a super-convergent meshless compu-

tational approach based on the differential quadrature method would be developed. **Figure 1E** represents the flowchart for the current work, the mathematical formulation and numerical results concerning which are presented in the following sections.

2. Mathematical Formulation for the Dynamics of Smart Twisted Beams

The bidirectionally functionally graded aluminum-Terfenol-D twisted beam is investigated in this study along with its geometric flaws, such as the porosity effect. **Figure 1A–D** depicts the geometric representation of the beam. Length, breadth, and thickness of the beam are correspondingly represented by the parameters L , B , and H . The beam maintains the same angular twist from its foundation to the tip. To further characterize the system, a Cartesian coordinate system is set up with the origin at the geometric centre of the leftmost part of the beam, the x -axis parallel

Table 1. Summary of key modeling assumptions used in the present formulation.

Aspect	Assumption/Justification
Beam theory	First-order shear deformation theory (FSDT) adopted; higher-order terms (TSDT) found negligible for present thickness ratios.
Material gradation	Bidirectional functional grading in thickness and longitudinal directions, modeled via power-law distribution.
Magnetostrictive layer	Terfenol-D layer modeled with linear magneto-mechanical coupling; effect of bias magnetic field included in constitutive matrix.
Deformation in $y-z$ plane	Neglected, as the beam is slender and primary deformation occurs in the $x-z$ bending plane.
Porosity	Uneven porosity considered through a porosity index (e_0); assumed to reduce stiffness but not mass density, uniformly.
Boundary conditions	Implemented through translational and rotational spring stiffness values; clamped, simply supported, and elastic supports obtained as limiting cases.
Damping	Velocity feedback included via equivalent viscous damping terms; viscoelastic supports modeled with dashpots.
Control strategy	Active vibration suppression modeled via velocity feedback from Terfenol-D patches; placement aligned with strain antinodes.

to the undeformed beam's centroidal axis, and the y - and z -axes parallel to the direction of the beam's breadth and thickness. For clarity and conciseness, the key modeling assumptions adopted in the present formulation are summarized in **Table 1**. These assumptions concerning the theoretical framework, material modeling choices, boundary condition treatments, and control strategies are also discussed later in more detail, as and if necessary.

2.1. Bidirectional Material Properties

In this work, the material composition is considered to vary along the axis, along the thickness, and also simultaneously along the thickness and the axis. The volume fraction of the ceramic according to the power law is defined as:

$$V_c = \left(\frac{1}{2} + \frac{z}{h}\right)^m \left(\frac{1}{2} + \frac{x}{L}\right)^n \quad (1)$$

where, m and n are non-negative variables which define the power law indices in transverse and axial directions respectively. Two types of porosity are investigated in this study considering even and uneven porosity distributions. The material properties of the bidirectional functionally graded even porosity can be defined as:

$$P(x, z) = P_m + (P_c - P_m) \left(\frac{1}{2} + \frac{z}{h}\right)^m \left(\frac{1}{2} + \frac{x}{L}\right)^n - \frac{\alpha}{2} (P_c + P_m) \quad (2)$$

where, z denotes the distance from the neutral axis of beams and α is the porosity volume fraction. The material properties for the uneven porosity distribution can be expressed as:

$$P(x, z) = P_m + (P_c - P_m) \left(\frac{1}{2} + \frac{z}{h}\right)^m \left(\frac{1}{2} + \frac{x}{L}\right)^n - \frac{\alpha}{2} (P_c + P_m) \left(1 - \frac{2|z|}{h}\right) \quad (3)$$

2.2. Displacement Components

The displacement field is represented as

$$u(x, y, z, t) = u_0(x, t) - z\theta(x, t) + \frac{4C_1}{3h^2} z^3 \left[\theta(x, t) - \frac{\partial w_0(x, t)}{\partial x} \right]$$

$$- \gamma \phi(x, t) + \frac{4C_1}{3b^2} \gamma^3 \left[\phi(x, t) - \frac{\partial v_0(x, t)}{\partial x} \right] \quad (4)$$

$$v(x, y, z, t) = v_0(x, t) \quad (5)$$

$$w(x, y, z, t) = w_0(x, t) \quad (6)$$

where $u(x, t)$, $v(x, t)$, and $w(x, t)$ are the displacement components of the point (x, y) at the mid-plane of the beam cross-section. The parameters, $\theta(x, t)$ and $\phi(x, t)$ are the bending rotation of the beam cross-section about y -axis and z -axis, respectively. One can express the displacement relations as first order shear deformation theory (FSDT: $C_1 = 0$) and Reddy's third-order shear deformation theory (TSDT: $C_1 = 1$). Though we will not focus on obtaining any comparative numerical results concerning these theories, the flexibility of the presented formulation will enable interested researchers to investigate the influence of shear deformation on the dynamic behavior of the twisted beam and compare the predictions of these two widely used theories. The nonzero strain-displacement relations are given as

$$\begin{aligned} \epsilon_{xx} = & \frac{\partial u}{\partial x} - \gamma \left(\frac{\partial \phi}{\partial x} + Q\theta \right) - z \left(\frac{\partial \theta}{\partial x} - Q\phi \right) \\ & + \frac{4C_1}{h^2} \left[Qz^2 \gamma \left(\theta - \frac{\partial w_0}{\partial x} \right) + \frac{z^3}{3} \left(\frac{\partial \theta}{\partial x} - \frac{\partial^2 w_0}{\partial x^2} \right) \right. \\ & \left. - \alpha^2 Q \gamma^2 z \left(\phi - \frac{\partial v}{\partial x} \right) + \frac{\alpha^2 z^3}{3} \left(\frac{\partial \phi}{\partial x} - \frac{\partial^2 v}{\partial x^2} \right) \right] \quad (7) \end{aligned}$$

$$\epsilon_{xy} = \epsilon_{yx} = \left(\frac{1}{2} - \frac{2C_1}{b^2} \gamma^2 \right) \left(\frac{\partial v}{\partial x} - \phi \right) \quad (8)$$

$$\epsilon_{xz} = \epsilon_{zx} = \left(\frac{1}{2} - \frac{2C_1}{h^2} z^2 \right) \left(\frac{\partial w_0}{\partial x} - \theta \right) \quad (9)$$

where, $Q = \frac{d\phi}{dx}$ and $\alpha = \frac{h}{b}$.

2.3. Constitutive Relations

The constitutive relations for the bidirectional functionally graded aluminum-Terfenol-D beam are given as:

$$\sigma_{xx} = \bar{Q}_{11}^{(k)} \epsilon_{xx}, \quad \sigma_{xy} = \bar{Q}_{55}^{(k)} \epsilon_{xy}, \quad \sigma_{xz} = \bar{Q}_{44}^{(k)} \epsilon_{xz} \quad (10)$$

where, $\bar{Q}_{11}^{(k)}$, $\bar{Q}_{55}^{(k)}$, and $\bar{Q}_{44}^{(k)}$ are the transformed stiffnesses of Terfenol-D layered functionally graded twisted beam. The calculation of these transformed stiffness can be found in literature.^[73] The constitutive relation for Terfenol-D material is given as:

$$\sigma_{xx} = Q^{(m)} \epsilon_{xx} - d^{(m)} H \quad (11)$$

where, H , $d^{(m)}$ are the magnetic field intensity and magneto-mechanical coupling coefficient of Terfenol-D layer.

2.4. Velocity Feedback Control

In order to control the free vibration of bidirectional functionally graded aluminium-Terfenol-D twisted beams, we have considered the velocity proportional closed loop feedback control approach. The magnetic field intensity H is expressed as:

$$H(x, t) = k_c I(x, t) \quad (12)$$

where, k_c and $I(x, t)$ are the coil constant meant to produce the required magnetic field intensity and current supplied to coils. The expression for the k_c and $I(x, t)$ can be written as:

$$k_c = \frac{n_c}{\sqrt{b_c^2 + 4r_c^2}} \quad \text{and} \quad I(x, t) = C(t) \frac{\partial w_0}{\partial t} \quad (13)$$

2.5. Equation of Motion

The strain energy of the bidirectional functionally graded aluminium-Terfenol-D beam can be written as:

$$U = \frac{1}{2} \int_0^L \int_{-\frac{h}{2}}^{\frac{h}{2}} \int_{-\frac{b}{2}}^{\frac{b}{2}} (\sigma_{xx} \epsilon_{xx} + 2\sigma_{xy} \epsilon_{xy} + 2\sigma_{xz} \epsilon_{xz}) dydzdx \quad (14)$$

In the context of the above equation, it may be noted that the current study primarily focuses on the transverse response of the twisted beam. To capture the dominant deformation modes relevant to this focus, the strain energy expression incorporates three key terms: *Bending in the x-z plane*: This term accounts for the primary bending deformation of the beam in the plane perpendicular to the twist axis, which is crucial for understanding transverse vibrations. *Axial deformation*: This term considers the axial elongation or compression of the beam fibers, which can significantly influence the overall dynamic behavior. *Shear deformation*: This term accounts for the transverse shear deformation of the beam, which becomes important for thicker beams or when higher-order effects are considered. *Justification for neglecting y-z plane Deformation*: The effect of deformation in the y-z plane is not explicitly considered in this model. This simplification is based on the following assumption of dominant deformation modes to achieve working simplification. The primary focus of this study is on the transverse vibrations of the beam, which are predominantly driven by bending in the x-z plane. Deformation in the y-z plane is expected to have a secondary or negligible influence on the overall dynamic response within the scope of this investigation. Though it will be more accurate, including deformation in

the y-z plane would significantly increase the complexity of the governing equations and the subsequent analysis. This simplification allows to carry out a more focused and computationally efficient analysis of the dominant deformation modes. However, we note that the additional terms may be incorporated in future studies following the current computational framework, if necessary. The shear correction factor (k_s) accounts for the nonuniform distribution of transverse shear stresses across the thickness. In this study, $k_s = 5/6$ is adopted.

The kinetic energy of the Terfenol-D layered functionally graded beam can be written as:

$$\bar{K}E = \frac{1}{2} \int_0^T \int_0^L \int_A \rho \left(\left(\frac{\partial u}{\partial t} \right)^2 + \left(\frac{\partial v}{\partial t} \right)^2 + \left(\frac{\partial w}{\partial t} \right)^2 \right) dAdxdt \quad (15)$$

Now, one can expand the strain energy in the following form:

$$U = \frac{1}{2} \int_0^L \int_{-\frac{h}{2}}^{\frac{h}{2}} \int_{-\frac{b}{2}}^{\frac{b}{2}} \left\{ (\sigma_{xx} \epsilon_{xx} + 2\sigma_{xy} \epsilon_{xy} + 2\sigma_{xz} \epsilon_{xz}) \right\} dydzdx \quad (16)$$

$$U = \frac{1}{2} \int_0^L \left\{ \left[N_{xx} \frac{\partial u}{\partial x} - M_{xx1} \left(\frac{\partial \phi}{\partial x} + Q_{twist} \theta \right) - M_{xx2} \left(\frac{\partial \theta}{\partial x} - Q_{twist} \phi \right) + R_{xx3} \left(\theta - \frac{\partial w_0}{\partial x} \right) + R_{zzz} \left(\frac{\partial \theta}{\partial x} - \frac{\partial^2 w_0}{\partial x^2} \right) - R_{xyz} \left(\phi - \frac{\partial v}{\partial x} \right) + R_{zyy} \left(\frac{\partial \phi}{\partial x} - \frac{\partial^2 v}{\partial x^2} \right) \right] + \left(N_{xy} - M_{xy} \left(\frac{\partial v}{\partial x} - \phi \right) \right) + \left(N_{xz} - M_{xz} \left(\frac{\partial w}{\partial x} - \theta \right) \right) \right\} dx \quad (17)$$

where,

$$N_{xx} = \int_{-\frac{h}{2}}^{\frac{h}{2}} \int_{-\frac{b}{2}}^{\frac{b}{2}} \sigma_{xx} dydz \quad (18)$$

$$N_{xx} = \int_{-\frac{h}{2}}^{\frac{h}{2}} \int_{-\frac{b}{2}}^{\frac{b}{2}} Q_{11} \epsilon_{xx} dydz \quad (19)$$

$$N_{xx} = \int_{-\frac{h}{2}}^{\frac{h}{2}} \int_{-\frac{b}{2}}^{\frac{b}{2}} Q_{11} \left\{ \frac{\partial u}{\partial x} - \gamma \left(\frac{\partial \phi}{\partial x} + Q_{twist} \theta \right) - z \left(\frac{\partial \theta}{\partial x} - Q_{twist} \phi \right) + \frac{4C_1}{h^2} \left[Qz^2 \gamma \left(\theta - \frac{\partial w_0}{\partial x} \right) + \frac{z^3}{3} \left(\frac{\partial \theta}{\partial x} - \frac{\partial^2 w_0}{\partial x^2} \right) - \alpha^2 Q \gamma^2 z \left(\phi - \frac{\partial v}{\partial x} \right) + \frac{\alpha^2 z^3}{3} \left(\frac{\partial \phi}{\partial x} - \frac{\partial^2 v}{\partial x^2} \right) \right] \right\} dydz \quad (20)$$

$$N_{xx} = A_{00} \frac{\partial u}{\partial x} - A_{01} \left(\frac{\partial \phi}{\partial x} + Q_{twist} \theta \right) - A_{10} \left(\frac{\partial \theta}{\partial x} - Q_{twist} \phi \right) + \frac{4C_1 Q}{h^2} A_{21} \left(\theta - \frac{\partial w_0}{\partial x} \right) + \frac{4C_1}{3h^2} A_{30} \left(\frac{\partial \theta}{\partial x} - \frac{\partial^2 w_0}{\partial x^2} \right) - \frac{4C_1 Q_{twist}}{b^2} A_{12} \left(\phi - \frac{\partial v}{\partial x} \right) + \frac{4C_1}{3b^2} A_{03} \left(\frac{\partial \phi}{\partial x} - \frac{\partial^2 v}{\partial x^2} \right) \quad (21)$$

$$\mathbf{M}_{xx1} = \int_{-\frac{h}{2}}^{\frac{h}{2}} \int_{-\frac{b}{2}}^{\frac{b}{2}} \sigma_{xx} Y dy dz \quad (22) \quad \mathbf{R}_{xzz} = \left(\frac{4C_1}{3h^2} \right) \int_{-\frac{h}{2}}^{\frac{h}{2}} \int_{-\frac{b}{2}}^{\frac{b}{2}} Q_{11} \epsilon_{xx} z^3 dy dz \quad (32)$$

$$\mathbf{M}_{xx1} = \int_{-\frac{h}{2}}^{\frac{h}{2}} \int_{-\frac{b}{2}}^{\frac{b}{2}} Q_{11} \epsilon_{xx} Y dy dz \quad (23) \quad \mathbf{R}_{xzz} = \left(\frac{4C_1}{3h^2} \right) \left[A_{30} \frac{\partial u}{\partial x} - A_{31} \left(\frac{\partial \phi}{\partial x} + Q_{twist} \theta \right) \right.$$

$$\begin{aligned} \mathbf{M}_{xx1} = & A_{01} \frac{\partial u}{\partial x} - A_{02} \left(\frac{\partial \phi}{\partial x} + Q_{twist} \theta \right) - A_{11} \left(\frac{\partial \theta}{\partial x} - Q_{twist} \phi \right) \\ & + \frac{4C_1 Q_{twist}}{h^2} A_{22} \left(\theta - \frac{\partial w_0}{\partial x} \right) + \frac{4C_1}{3h^2} A_{31} \left(\frac{\partial \theta}{\partial x} - \frac{\partial^2 w_0}{\partial x^2} \right) \\ & - \frac{4C_1 Q_{twist}}{b^2} A_{13} \left(\phi - \frac{\partial v}{\partial x} \right) + \frac{4C_1}{3b^2} A_{04} \left(\frac{\partial \phi}{\partial x} - \frac{\partial^2 v}{\partial x^2} \right) \quad (24) \end{aligned}$$

$$\begin{aligned} & - A_{40} \left(\frac{\partial \theta}{\partial x} - Q_{twist} \phi \right) + \frac{4C_1 Q_{twist}}{h^2} A_{51} \left(\theta - \frac{\partial w_0}{\partial x} \right) \\ & + \frac{4C_1}{3h^2} A_{60} \left(\frac{\partial \theta}{\partial x} - \frac{\partial^2 w_0}{\partial x^2} \right) - \frac{4C_1 Q_{twist}}{b^2} A_{42} \left(\phi - \frac{\partial v}{\partial x} \right) \\ & + \left. \frac{4C_1}{3b^2} A_{33} \left(\frac{\partial \phi}{\partial x} - \frac{\partial^2 v}{\partial x^2} \right) - \epsilon \frac{\partial w_0}{\partial t} \right] \quad (33) \end{aligned}$$

$$\mathbf{M}_{xx2} = \int_{-\frac{h}{2}}^{\frac{h}{2}} \int_{-\frac{b}{2}}^{\frac{b}{2}} \sigma_{xx} z dy dz \quad (25) \quad \mathbf{R}_{xyz} = \left(\frac{4C_1 Q_{twist}}{b^2} \right) \int_{-\frac{h}{2}}^{\frac{h}{2}} \int_{-\frac{b}{2}}^{\frac{b}{2}} \sigma_{xx} Y^2 z dy dz \quad (34)$$

$$\mathbf{M}_{xx2} = \int_{-\frac{h}{2}}^{\frac{h}{2}} \int_{-\frac{b}{2}}^{\frac{b}{2}} Q_{11} \epsilon_{xx} z dy dz \quad (26) \quad \mathbf{R}_{xyz} = \left(\frac{4C_1 Q_{twist}}{b^2} \right) \int_{-\frac{h}{2}}^{\frac{h}{2}} \int_{-\frac{b}{2}}^{\frac{b}{2}} Q_{11} \epsilon_{xx} Y^2 z dy dz \quad (35)$$

$$\begin{aligned} \mathbf{M}_{xx2} = & A_{10} \frac{\partial u}{\partial x} - A_{11} \left(\frac{\partial \phi}{\partial x} + Q_{twist} \theta \right) - A_{20} \left(\frac{\partial \theta}{\partial x} - Q_{twist} \phi \right) \\ & + \frac{4C_1 Q_{twist}}{h^2} A_{31} \left(\theta - \frac{\partial w_0}{\partial x} \right) + \frac{4C_1}{3h^2} A_{40} \left(\frac{\partial \theta}{\partial x} - \frac{\partial^2 w_0}{\partial x^2} \right) \\ & - \frac{4C_1 Q_{twist}}{b^2} A_{22} \left(\phi - \frac{\partial v}{\partial x} \right) + \frac{4C_1}{3b^2} A_{13} \left(\frac{\partial \phi}{\partial x} - \frac{\partial^2 v}{\partial x^2} \right) - \beta \frac{\partial w_0}{\partial t} \quad (27) \end{aligned}$$

$$\begin{aligned} \mathbf{R}_{xzz} = & \left(\frac{4C_1 Q_{twist}}{b^2} \right) \left[A_{12} \frac{\partial u}{\partial x} - A_{13} \left(\frac{\partial \phi}{\partial x} + Q_{twist} \theta \right) \right. \\ & - A_{22} \left(\frac{\partial \theta}{\partial x} - Q_{twist} \phi \right) + \frac{4C_1 Q_{twist}}{h^2} A_{33} \left(\theta - \frac{\partial w_0}{\partial x} \right) \\ & + \frac{4C_1}{3h^2} A_{42} \left(\frac{\partial \theta}{\partial x} - \frac{\partial^2 w_0}{\partial x^2} \right) - \frac{4C_1 Q_{twist}}{b^2} A_{24} \left(\phi - \frac{\partial v}{\partial x} \right) \\ & + \left. \frac{4C_1}{3b^2} A_{15} \left(\frac{\partial \phi}{\partial x} - \frac{\partial^2 v}{\partial x^2} \right) \right] \quad (36) \end{aligned}$$

$$\mathbf{R}_{xzy} = \left(\frac{4C_1 Q_{twist}}{h^2} \right) \int_{-\frac{h}{2}}^{\frac{h}{2}} \int_{-\frac{b}{2}}^{\frac{b}{2}} \sigma_{xx} z^2 y dy dz \quad (28)$$

$$\mathbf{R}_{xzy} = \left(\frac{4C_1 Q_{twist}}{h^2} \right) \int_{-\frac{h}{2}}^{\frac{h}{2}} \int_{-\frac{b}{2}}^{\frac{b}{2}} Q_{11} \epsilon_{xx} z^2 y dy dz \quad (29)$$

$$\begin{aligned} \mathbf{R}_{xzy} = & \left(\frac{4C_1 Q_{twist}}{h^2} \right) \left[A_{21} \frac{\partial u}{\partial x} - A_{22} \left(\frac{\partial \phi}{\partial x} + Q_{twist} \theta \right) \right. \\ & - A_{31} \left(\frac{\partial \theta}{\partial x} - Q_{twist} \phi \right) + \frac{4C_1 Q_{twist}}{h^2} A_{42} \left(\theta - \frac{\partial w_0}{\partial x} \right) \\ & + \frac{4C_1}{3h^2} A_{51} \left(\frac{\partial \theta}{\partial x} - \frac{\partial^2 w_0}{\partial x^2} \right) - \frac{4C_1 Q_{twist}}{b^2} A_{33} \left(\phi - \frac{\partial v}{\partial x} \right) \\ & + \left. \frac{4C_1}{3b^2} A_{24} \left(\frac{\partial \phi}{\partial x} - \frac{\partial^2 v}{\partial x^2} \right) \right] \quad (30) \end{aligned}$$

$$\mathbf{R}_{xzz} = \left(\frac{4C_1}{3h^2} \right) \int_{-\frac{h}{2}}^{\frac{h}{2}} \int_{-\frac{b}{2}}^{\frac{b}{2}} \sigma_{xx} z^3 dy dz \quad (31)$$

$$\mathbf{R}_{zyy} = \left(\frac{4C_1}{3b^2} \right) \int_{-\frac{h}{2}}^{\frac{h}{2}} \int_{-\frac{b}{2}}^{\frac{b}{2}} \sigma_{xx} Y^3 dy dz \quad (37)$$

$$\mathbf{R}_{zyy} = \left(\frac{4C_1}{3b^2} \right) \int_{-\frac{h}{2}}^{\frac{h}{2}} \int_{-\frac{b}{2}}^{\frac{b}{2}} Q_{11} \epsilon_{xx} Y^3 dy dz \quad (38)$$

$$\begin{aligned} \mathbf{R}_{zyy} = & \left(\frac{4C_1}{3b^2} \right) \left[A_{03} \frac{\partial u}{\partial x} - A_{04} \left(\frac{\partial \phi}{\partial x} + Q_{twist} \theta \right) \right. \\ & - A_{13} \left(\frac{\partial \theta}{\partial x} - Q_{twist} \phi \right) + \frac{4C_1 Q_{twist}}{h^2} A_{24} \left(\theta - \frac{\partial w_0}{\partial x} \right) \\ & + \frac{4C_1}{3h^2} A_{33} \left(\frac{\partial \theta}{\partial x} - \frac{\partial^2 w_0}{\partial x^2} \right) - \frac{4C_1 Q_{twist}}{b^2} A_{15} \left(\phi - \frac{\partial v}{\partial x} \right) \\ & + \left. \frac{4C_1}{3b^2} A_{06} \left(\frac{\partial \phi}{\partial x} - \frac{\partial^2 v}{\partial x^2} \right) \right] \quad (39) \end{aligned}$$

$$\mathbf{N}_{xy} = \int_{-\frac{h}{2}}^{\frac{h}{2}} \int_{-\frac{b}{2}}^{\frac{b}{2}} \sigma_{xy} dy dz \quad (40)$$

$$N_{xy} = \int_{-\frac{h}{2}}^{\frac{h}{2}} \int_{-\frac{b}{2}}^{\frac{b}{2}} Q_{55} \epsilon_{xy} dy dz \quad (41)$$

$$N_{xy} = \int_{-\frac{h}{2}}^{\frac{h}{2}} \int_{-\frac{b}{2}}^{\frac{b}{2}} Q_{55} \left(\frac{1}{2} - \frac{2C_1}{b^2} y^2 \right) \left(\frac{\partial v}{\partial x} - \phi \right) dy dz \quad (42)$$

$$N_{xy} = \frac{1}{2} \int_{-\frac{h}{2}}^{\frac{h}{2}} \int_{-\frac{b}{2}}^{\frac{b}{2}} Q_{55} \left(1 - \frac{4C_1}{b^2} y^2 \right) \left(\frac{\partial v}{\partial x} - \phi \right) dy dz \quad (43)$$

$$N_{xy} = \frac{1}{2} \int_{-\frac{h}{2}}^{\frac{h}{2}} \int_{-\frac{b}{2}}^{\frac{b}{2}} \left(Q_{55} - \frac{4C_1}{b^2} Q_{55} y^2 \right) \left(\frac{\partial v}{\partial x} - \phi \right) dy dz \quad (44)$$

$$N_{xy} = \frac{1}{2} \left(D_{00} - \frac{4C_1}{b^2} D_{02} \right) \left(\frac{\partial v}{\partial x} - \phi \right) \quad (45)$$

$$M_{xy} = \int_{-\frac{h}{2}}^{\frac{h}{2}} \int_{-\frac{b}{2}}^{\frac{b}{2}} \sigma_{xy} y^2 dy dz \quad (46)$$

$$M_{xy} = \int_{-\frac{h}{2}}^{\frac{h}{2}} \int_{-\frac{b}{2}}^{\frac{b}{2}} Q_{55} \left\{ \left(\frac{1}{2} - \frac{2C_1}{b^2} y^2 \right) \left(\frac{\partial v}{\partial x} - \phi \right) \right\} y^2 dy dz \quad (47)$$

$$M_{xy} = \frac{1}{2} \left(D_{02} - \frac{4C_1}{b^2} D_{04} \right) \left(\frac{\partial v}{\partial x} - \phi \right) \quad (48)$$

$$N_{xz} = \int_{-\frac{h}{2}}^{\frac{h}{2}} \int_{-\frac{b}{2}}^{\frac{b}{2}} \sigma_{xz} dy dz \quad (49)$$

$$N_{xz} = \frac{1}{2} \left(D_{00} - \frac{4C_1}{h^2} D_{20} \right) \left(\frac{\partial w_0}{\partial x} - \theta \right) \quad (50)$$

$$M_{xz} = \int_{-\frac{h}{2}}^{\frac{h}{2}} \int_{-\frac{b}{2}}^{\frac{b}{2}} \sigma_{xz} z^2 dy dz \quad (51)$$

$$M_{xz} = \frac{1}{2} \left(D_{20} - \frac{4C_1}{b^2} D_{40} \right) \left(\frac{\partial v}{\partial x} - \phi \right) \quad (52)$$

The two stiffness coefficients presented in the above terms are given as:

$$B_{pq} = \int_{-\frac{h}{2}}^{\frac{h}{2}} \int_{-\frac{b}{2}}^{\frac{b}{2}} Q_{11}(z) z^p y^q dy dz \quad p, q = 0, 1, 2, 3, 4 \quad (53)$$

$$D_{kl} = \int_{-\frac{h}{2}}^{\frac{h}{2}} \int_{-\frac{b}{2}}^{\frac{b}{2}} Q_{55}(z) z^k y^l dy dz \quad k, l = 0, 1, 2, 3, 4 \quad (54)$$

$$\beta = \int_{-\frac{h}{2}}^{\frac{h}{2}} k_c C(t) Q_{11}^{(m)} d^{(m)} z dz \quad (55)$$

$$\epsilon = \int_{-\frac{h}{2}}^{\frac{h}{2}} k_c C(t) Q_{11}^{(m)} d^{(m)} z^3 dz \quad (56)$$

One can write the kinetic energy of the Terfenol-D layered functionally graded twisted beam as:

$$\begin{aligned} \bar{K}E = & \frac{1}{2} \int_0^L \left[I_{00} \left(\frac{\partial u}{\partial t} \right)^2 + I_{20} \left(\frac{\partial \theta}{\partial t} \right)^2 + I_{60} \frac{16C_1}{9h^2} \left(\frac{\partial \theta}{\partial t} - \frac{\partial^2 w_0}{\partial t \partial x} \right) \right. \\ & + I_{02} \left(\frac{\partial \phi}{\partial t} \right) + I_{06} \frac{16C_1}{9b^4} \left[\frac{\partial \phi}{\partial t} - \frac{\partial^2 v}{\partial t \partial x} \right]^2 - 2I_{10} \left(\frac{\partial u}{\partial t} \right) \left(\frac{\partial \theta}{\partial t} \right) \\ & + I_{30} \frac{8C_1}{3h^2} \left(\frac{\partial u}{\partial t} \right) \left(\frac{\partial \theta}{\partial t} - \frac{\partial^2 w_0}{\partial t \partial x} \right) - 2I_{01} \left(\frac{\partial u}{\partial t} \right) \left(\frac{\partial \phi}{\partial t} \right) \\ & + I_{03} \frac{8C_1}{3b^2} \left(\frac{\partial u}{\partial t} \right) \left(\frac{\partial \phi}{\partial t} - \frac{\partial^2 v}{\partial t \partial x} \right) - I_{40} \frac{8C_1}{3h^2} \frac{\partial \theta}{\partial t} \left(\frac{\partial \theta}{\partial t} - \frac{\partial^2 w_0}{\partial t \partial x} \right) \\ & + 2I_{11} \left(\frac{\partial \theta}{\partial t} \right) \left(\frac{\partial \phi}{\partial t} \right) - I_{13} \frac{8C_1}{3b^2} \left(\frac{\partial \theta}{\partial t} \right) \left(\frac{\partial \phi}{\partial t} - \frac{\partial^2 v}{\partial t \partial x} \right) \\ & - I_{31} \frac{8C_1}{3h^2} \left(\frac{\partial \phi}{\partial t} \right) \left(\frac{\partial \theta}{\partial t} - \frac{\partial^2 w_0}{\partial t \partial x} \right) I_{33} \frac{32C_1}{9h^2 b^2} \left(\frac{\partial \theta}{\partial t} - \frac{\partial^2 w_0}{\partial t \partial x} \right) \\ & \times \left(\frac{\partial \phi}{\partial t} - \frac{\partial^2 v}{\partial t \partial x} \right) - I_{04} \frac{8C_1}{3b^2} \left(\frac{\partial \phi}{\partial t} \right) \left(\frac{\partial \phi}{\partial t} - \frac{\partial^2 v}{\partial t \partial x} \right) \\ & \left. + I_{00} \left(\frac{\partial v}{\partial t} \right)^2 + I_{00} \left(\frac{\partial w_0}{\partial t} \right)^2 \right] dx \quad (57) \end{aligned}$$

where, inertia coefficients in the above equation are defined as:

$$I_{pq} = \int_{-\frac{h}{2}}^{\frac{h}{2}} \int_{-\frac{b}{2}}^{\frac{b}{2}} \rho z^p y^q dz dy \quad p, q = 0, 1, 2, 3, 4, 5, 6 \quad (58)$$

The governing equation of bidirectional functionally graded aluminium-Terfenol-D twisted beams can be obtained by means of the Hamilton's principle as:

$$\delta \int_{t_1}^{t_2} [T(t) - U(t) + W_{ext}(t)] dt = 0 \quad (59)$$

By performing the variational operations, integrating the appropriate terms by parts and collecting the coefficients of δu , $\delta \phi$, $\delta \theta$, δv , and δw_0 , the variationally consistent equation of motion for first order shear deformation theory (FSDT) in terms of stress resultant can be written as:

$$\delta u = 0 \Rightarrow \frac{\partial N_{xx}}{\partial x} + I_{00} \frac{\partial^2 u}{\partial t^2} - 2I_{10} \frac{\partial^2 \theta}{\partial t^2} - 2I_{01} \frac{\partial^2 \phi}{\partial t^2} = 0 \quad (60)$$

$$\delta v = 0 \Rightarrow \frac{\partial N_{xy}}{\partial x} + I_{00} \frac{\partial^2 v}{\partial t^2} = 0 \quad (61)$$

$$\delta w = 0 \Rightarrow \frac{\partial N_{xz}}{\partial x} + I_{00} \frac{\partial^2 w}{\partial t^2} = 0 \quad (62)$$

$$\begin{aligned} \delta \theta \Rightarrow & -M_{xx} Q_{wist} - \frac{\partial M_{xy}}{\partial x} - N_{xz} + I_{20} \frac{\partial^2 \theta}{\partial t^2} \\ & - 2I_{10} \frac{\partial^2 u}{\partial t^2} + 2I_{11} \frac{\partial^2 \phi}{\partial t^2} = 0 \quad (63) \end{aligned}$$

$$\delta\phi := -\frac{\partial M_{xx}}{\partial x} + M_{xy}Q_{\text{twist}} - N_{xy} + I_{02}\frac{\partial^2\phi}{\partial t^2} - 2I_{01}\frac{\partial^2 u}{\partial t^2} + 2I_{11}\frac{\partial^2\theta}{\partial t^2} = 0 \quad (64)$$

Expanding and substituting the stress resultants in the governing equations based on FSDT, we get:

$$B_{00}\frac{\partial^2 u}{\partial x^2} - B_{01}Q_{\text{twist}}\frac{\partial\theta}{\partial x} - B_{01}\frac{\partial^2\phi}{\partial x^2} - B_{10}\frac{\partial^2\theta}{\partial x^2} + B_{10}Q_{\text{twist}}\frac{\partial\phi}{\partial x} + I_{00}\frac{\partial^2 u}{\partial t^2} - 2I_{10}\frac{\partial^2\theta}{\partial t^2} - 2I_{01}\frac{\partial^2\phi}{\partial t^2} = 0 \quad (65)$$

$$D_{00}\frac{\partial^2 v}{\partial x^2} - D_{00}\frac{\partial\phi}{\partial x} + I_{00}\frac{\partial^2 v}{\partial t^2} = 0 \quad (66)$$

$$D_{00}k_s\frac{\partial^2 w}{\partial x^2} - D_{00}k_s\frac{\partial\theta}{\partial x} + I_{00}\frac{\partial^2 w}{\partial t^2} = 0 \quad (67)$$

$$-Q_{\text{twist}}B_{10}\frac{\partial u}{\partial x} + B_{11}Q_{\text{twist}}\theta + B_{11}Q_{\text{twist}}\frac{\partial\phi}{\partial x} + Q_{\text{twist}}B_{20}\frac{\partial\theta}{\partial x} - B_{20}Q_{\text{twist}}\phi - Q_{\text{twist}}\beta\frac{\partial^2 w}{\partial t\partial x} - B_{01}\frac{\partial^2 u}{\partial x^2} + B_{02}Q_{\text{twist}}\frac{\partial\theta}{\partial x} + B_{02}\frac{\partial^2\phi}{\partial x^2} + B_{11}\frac{\partial^2\theta}{\partial x^2} - B_{11}Q_{\text{twist}}\frac{\partial\phi}{\partial x} - D_{00}k_s\frac{\partial w}{\partial x} + D_{00}k_s\theta + I_{20}\frac{\partial^2\theta}{\partial t^2} - 2I_{10}\frac{\partial^2 u}{\partial t^2} + 2I_{11}\frac{\partial^2\phi}{\partial t^2} = 0 \quad (68)$$

$$-B_{10}\frac{\partial^2 u}{\partial x^2} + B_{11}Q_{\text{twist}}\frac{\partial\theta}{\partial x} + B_{11}\frac{\partial^2\phi}{\partial x^2} + B_{20}\frac{\partial^2\theta}{\partial x^2} - B_{20}Q_{\text{twist}}\frac{\partial\phi}{\partial x} - \beta\frac{\partial^3 w}{\partial x^2\partial t} + B_{01}Q_{\text{twist}}\frac{\partial u}{\partial x} - B_{02}Q_{\text{twist}}\theta - B_{02}Q_{\text{twist}}\frac{\partial\phi}{\partial x} - B_{11}Q_{\text{twist}}\frac{\partial\theta}{\partial x} + B_{11}Q_{\text{twist}}^2\theta - D_{00}\frac{\partial v}{\partial x} + D_{00}\phi + I_{02}\frac{\partial^2\phi}{\partial t^2} - 2I_{01}\frac{\partial^2 u}{\partial t^2} + 2I_{11}\frac{\partial^2\theta}{\partial t^2} = 0 \quad (69)$$

The coefficients B_{ij} , D_{00} and I_{ij} are structural parameters, B_{ij} collect the elastic (extensional-bending-torsion-shear) stiffness's arising from the bidirectional functional gradation; D_{00} is the shear/warping stiffness (scaled by the shear-correction factor k_s); and I_{ij} are the consistent inertia terms, including cross-inertias that couple axial, bending, and torsional accelerations. The symbols Q_{twist} and β carry the actuation/control and twist couplings: Q_{twist} is the geometry-induced coupling coefficient produced by the beam's twist (it projects local bending/torsion into the global axial/warping directions and vice versa), and β scales the magnetostrictive control (velocity-like) feedback injected by the Terfenol-D layer(s). With this in view:

1. The first equation (axial field u) shows extensional stiffness B_{00} with twist-mediated couplings Q ($\partial\theta/\partial x$, $\partial\phi/\partial x$) and curvature couplings $\partial^2\theta/\partial x^2$, $\partial^2\phi/\partial x^2$, while I_{00} , I_{10} , I_{01} reveal

how axial inertia is cross-coupled to bending and torsional accelerations, an effect influenced by gradation and twist.

2. The second equation (interpreting $\partial^2 v/\partial x^2$) links in-plane lateral motion v to torsion via $\partial\phi/\partial x$; D_{00} provides the shear/warping resistance and I_{00} the lateral inertia.
3. The third equation (transverse motion w) couples out-of-plane displacement to the bending rotation θ through the shear channel $D_{00}k_s$, again with I_{00} providing inertia.
4. The fourth equation (bending rotation θ) gathers bending and torsion curvatures (B_{11} , B_{20} , B_{02}) and their twist-weighted projections through Q_{twist} ; the terms $-Q_{\text{twist}}\beta\partial^2 w/(\partial t\partial x)$ and $-D_{00}k_s\partial w/\partial x + D_{00}k_s\theta$ show how magnetostrictive control and shear flexibility inject (or dissipate) rotational power, while I_{20} , I_{10} , I_{11} set the effective rotational inertia.
5. The fifth equation (torsional rotation ϕ) mirrors this structure for twist: torsional/bending curvatures and their Q_{twist} -weighted couplings appear with B_{20} , B_{11} , B_{02} ; $-\beta\partial^3 w/(\partial x^2\partial t)$ is the magnetostrictive torque-like control channel; and the $\pm Q_{\text{twist}}^2$ terms (e.g., $-B_{02}Q_{\text{twist}}^2\theta$, $+B_{11}Q_{\text{twist}}^2\theta$) quantify second-order twist amplifications that redistribute stiffness between bending and torsion.

Collectively, these equations show that: i) structural gradation tunes the baseline stiffness and inertia maps, ii) twist (Q_{twist}) creates strong geometry-based projections that entangle axial, bending, shear, and torsion, and iii) magnetostriction (β) supplies an active pathway to inject damping/control work, most directly into bending and torsional channels via $w - \theta - \phi$ couplings, enabling targeted suppression and tuning of the global dynamic response.

2.6. Addition of Extra Term Due to Rotation

The governing equation requires additional components to account for the centrifugal stiffness of the beam and the rotational speed Ω due to the angular rotation of the beam. The centrifugal stiffening is given by

$$P(z) = \int_l^z \rho A \Omega^2 (r + z) dz \quad (70)$$

This term can be added to the overall stiffness of the twisted beam. Here, r is the offset length between Terfenol-D beam and rotating hub, l is the length of twisted beam, and ρ represents the density of beam material.

3. Meshless Differential Quadrature Based Numerical Solution Scheme

In order to solve the governing equation of free vibration for imperfect bidirectional functionally graded aluminum-Terfenol-D twisted beams, differential quadrature method is implemented here. To analyse the natural frequency, the following expressions are assumed.

$$u(x, y, z, t) = U(x, y, z) \exp^{i\omega t} \quad (71)$$

$$v(x, y, z, t) = V(x, y, z) \exp^{i\omega t} \quad (72)$$

$$w(x, y, z, t) = W(x, y, z) \exp^{i\omega t} \quad (73)$$

$$\theta(x, y, z, t) = \Theta(x, y, z) \exp^{i\omega t} \quad (74)$$

$$\phi(x, y, z, t) = \Phi(x, y, z) \exp^{i\omega t} \quad (75)$$

where, $U(x, y, z)$, $V(x, y, z)$, $W(x, y, z)$, $\Theta(x, y, z)$, and $\Phi(x, y, z)$ represent the mode shapes. Governing equations can be written in the analog differential quadrature form as:

$$\begin{aligned} & B_{00} \sum_{j=1}^n A_{ij}^{(2)} U_j - B_{01} Q_{\text{twist}} \sum_{j=1}^n A_{ij}^{(1)} \Theta_j - B_{01} \sum_{j=1}^n A_{ij}^{(2)} \Phi_j \\ & - B_{10} \sum_{j=1}^n A_{ij}^{(2)} \Theta_j + B_{10} Q_{\text{twist}} \sum_{j=1}^n A_{ij}^{(1)} \Phi_j + I_{00} U_i \lambda^2 \\ & - 2I_{10} \Theta_i \lambda^2 - 2I_{01} \Phi_i \lambda^2 = 0 \end{aligned} \quad (76)$$

$$D_{00} \sum_{j=1}^n A_{ij}^{(2)} V_j - D_{00} \sum_{j=1}^n A_{ij}^{(1)} \Phi_j + I_{00} V_i \lambda^2 = 0 \quad (77)$$

$$D_{00} k_s \sum_{j=1}^n A_{ij}^{(2)} W_j - D_{00} k_s \sum_{j=1}^n A_{ij}^{(1)} \Theta_j + I_{00} W_i \lambda^2 = 0 \quad (78)$$

$$\begin{aligned} & - Q_{\text{twist}} B_{10} \sum_{j=1}^n A_{ij}^{(1)} U_j + B_{11} Q_{\text{twist}} \Theta_j + B_{11} Q_{\text{twist}} \sum_{j=1}^n A_{ij}^{(1)} \Phi_j \\ & + Q_{\text{twist}} B_{20} \sum_{j=1}^n A_{ij}^{(1)} \Theta_j - B_{20} Q_{\text{twist}} \Phi_j - Q_{\text{twist}} \beta \sum_{j=1}^n A_{ij}^{(1)} W_j \lambda \\ & - B_{01} \sum_{j=1}^n A_{ij}^{(2)} U_j + B_{02} Q_{\text{twist}} \sum_{j=1}^n A_{ij}^{(1)} \Theta_j + B_{02} \sum_{j=1}^n A_{ij}^{(2)} \Phi_j \\ & + B_{11} \sum_{j=1}^n A_{ij}^{(2)} \Theta_j - B_{11} Q_{\text{twist}} \sum_{j=1}^n A_{ij}^{(1)} \Phi_j - D_{00} k_s \sum_{j=1}^n A_{ij}^{(1)} W_j \\ & + D_{00} k_s \Theta_j + I_{20} \Theta_i \lambda^2 - 2I_{10} U_i \lambda^2 + 2I_{11} \Phi_i \lambda^2 = 0 \end{aligned} \quad (79)$$

$$\begin{aligned} & - B_{10} \sum_{j=1}^n A_{ij}^{(2)} U_j + B_{11} Q_{\text{twist}} \sum_{j=1}^n A_{ij}^{(1)} \Theta_j + B_{11} \sum_{j=1}^n A_{ij}^{(2)} \Phi_j \\ & + B_{20} \sum_{j=1}^n A_{ij}^{(2)} \Theta_j - B_{20} Q_{\text{twist}} \sum_{j=1}^n A_{ij}^{(1)} \Phi_j - \beta \sum_{j=1}^n A_{ij}^{(2)} W_j \lambda \\ & + B_{01} Q_{\text{twist}} \sum_{j=1}^n A_{ij}^{(1)} U_j - B_{02} Q_{\text{twist}}^2 \Theta_j - B_{02} Q_{\text{twist}} \sum_{j=1}^n A_{ij}^{(1)} \Phi_j \\ & - B_{11} Q_{\text{twist}} \sum_{j=1}^n A_{ij}^{(1)} \Theta_j + B_{11} Q_{\text{twist}}^2 \Theta_j - D_{00} \sum_{j=1}^n A_{ij}^{(1)} V_j \\ & + D_{00} \Phi_j + I_{02} \Phi_i \lambda^2 - 2I_{01} U_i \lambda^2 + 2I_{11} \Theta_i \lambda^2 = 0 \end{aligned} \quad (80)$$

The above equations are written as

$$\{-[M] \lambda^2\} \{d\} + \{[Z] \lambda\} \{d\} + [\bar{S}] \{d\} = 0 \quad (81)$$

where,

$$[Z] = [C_{dd}] - [C_{db}] [S_{bb}]^{-1} [S_{bd}] \quad (82)$$

$$[\bar{S}] = [S_{dd}] - [S_{db}] [S_{bb}]^{-1} [S_{bd}] \quad (83)$$

Equation (81) is a non-standard eigenvalue equation. For a given frequency, it can be transformed equivalently into a standard form of eigenvalue equation as:

$$\left\{ \begin{bmatrix} 0 & I \\ Z & \bar{S} \end{bmatrix} - \begin{bmatrix} I & 0 \\ 0 & M \end{bmatrix} \lambda \right\} \begin{Bmatrix} d \\ \lambda d \end{Bmatrix} = 0 \quad (84)$$

where I is an identity matrix. $[\bar{S}]$, $[Z]$, and $[M]$ denote the structural stiffness, damping and mass matrix, respectively. $[M]$ is the matrix which contains the inertia terms from the governing differential equation. Reorganizing the matrices in Equation (84), one can get five sets of eigenvalues. The fundamental eigenvalue is thought to be the lowest one. The fundamental eigenpair corresponds to the lowest damped natural frequency. For a linear damped mode, the eigenvalues can be written as $\lambda = -\alpha \pm i\omega_d$, where α [s⁻¹] is the modal decay rate and ω_d [rad s⁻¹] is the damped natural frequency.

$$\omega_d = \sqrt{\omega_n^2 - \alpha^2}, \quad \omega_n = \sqrt{\alpha^2 + \omega_d^2} \quad (85)$$

The mode shapes can be plotted using the eigenvector.

The current study focuses on active vibration control of bidirectional functionally graded beams having twisted geometry along with viscoelastic boundary conditions, porosity variation, and the effect of designed Terfenol-D patch location. However, the limitations of the current approach in handling highly nonlinear scenarios may be noted. The future scope of further developments include potential extensions of the proposed computational approach to incorporate nonlinear effects, such as incorporating higher-order terms in the governing equations or employing more sophisticated numerical techniques, as well as magnetostrictive material nonlinearity and geometric nonlinearity.

4. Results and Discussion

This section presents numerical results concerning the free vibration and control of bidirectional functionally graded aluminium-Terfenol-D twisted beams. The proposed computational framework will be validated first with existing literature, followed by a comprehensive investigation on the dynamic behavior.

4.1. Validation of the Computational Framework

The current formulation and solution procedure is reduced to an isotropic beam with twist, and the numerical results are compared with literature as per availability.^[50,74] It may be noted that

Table 3. Convergence study for different grid points and validation of frequencies for twisted beams with literature considering $\beta = 0$. Note that β represents the magneto-mechanical coupling coefficient of the Terfenol-D actuator. This coefficient quantifies the strength of interaction between the magnetic field applied to Terfenol-D and the resulting mechanical strain, which directly influences the damping performance of the vibration control system. Here m_s represents the grid points, presenting a study on mesh convergence.

Modes	$m_s = 11$	$m_s = 27$	$m_s = 77$	$m_s = 100$	Ref. [74]	Ref. [50]	% Error with Ref. [74]
Mode 1	3.432	3.423	3.422	3.422	3.471	3.475	1.418
Mode 2	12.294	12.274	12.273	12.273	13.346	13.463	8.036
Mode 3	25.112	24.755	24.713	24.710	25.170	25.336	1.828
Mode 4	61.312	60.482	60.442	60.442	56.371	56.401	7.221
Mode 5	99.089	97.514	97.133	97.111	103.263	103.452	5.957

there hasn't been any prior research on the free vibration of a bidirectional functionally graded aluminum-Terfenol-D twisted beams. The convergence and validation of the differential quadrature method with first five mode frequencies are presented in Table 3 (for this the material properties of Table 2 are considered along with the geometrical parameters as: $L = 10$ m, $h = 10$ mm). It is observed that the natural frequencies obtained for twisted beam using differential quadrature method closely agree with the literature. Having adequate confidence on the developed computational framework, we further investigate the effect of a range of influencing parameters on the dynamic behavior.

Table 3 shows relatively higher percentage errors in vibration modes 2, 4, and 5, which can be attributed to the following reasons: 1) Theoretical framework differences: The reference by Banerjee^[74] employs the dynamic stiffness method, which is exact in the frequency domain and highly accurate for higher modes, while Adair and Jaeger^[50] use the modified Adomian decomposition method applied to a pre-twisted Euler–Bernoulli beam formulation. In contrast, our present approach is based on the generalized differential quadrature method (GDQM), which discretizes derivatives into weighted sums. Such methodological differences particularly influence higher modes where the sensitivity to formulation assumptions is greater. 2) Boundary condition implementation: Banerjee's dynamic stiffness framework^[74] enforces boundary conditions analytically, whereas in our GDQ-based scheme the clamped and simply supported conditions are approximated through weighting matrices. Small variations in constraint enforcement can significantly affect higher-order modes, which involve sharper curvature and higher strain energy concentrations near supports. 3) Numerical convergence sensitivity: Although convergence is demonstrated in Table 3, higher-order modes require denser grids and more refined shape

Table 2. Material Properties for the beam under consideration.^[75]

Parameters	Aluminium	Aluminium Oxide	Terfenol-D
Young's Modulus (Nm^{-2})	69×10^9	349.55×10^9	26.5×10^9
Poisson's Ratio	0.2892	0.260	0.30
Shear Modulus (Nm^{-2})	27×10^9	88×10^9	13.25×10^9
Density (kgm^{-3})	2900	3970	9250

Table 4. Imaginary component for varying vertical translational stiffness considering $K_L = 100000 \text{ Nm}^{-1}$, $K_{LT} = K_{RT} = 0 \text{ Nm}^{-1}$ and $C_L = C_R = C_{LT} = C_{RT} = 0 \text{ N-sm}^{-1}$, $m = n = 0.1$ and $\alpha = 0.1$.

K_R	$\phi = 40^\circ$	$\phi = 30^\circ$	$\phi = 20^\circ$	$\phi = 10^\circ$	$\phi = 0^\circ$
100000	118.3831	109.3057	87.7536	52.3032	42.4379
10000	118.3438	109.2723	87.7264	52.2813	42.4182
1000	117.9660	108.9482	86.4596	51.0652	41.2232
100	114.2574	105.4623	82.2643	49.1618	38.4103
10	100.6390	91.1956	71.2343	38.0319	26.0487
0	71.4636	62.2544	46.9092	22.5798	18.5324

functions to achieve the same accuracy as fundamental modes. The dynamic stiffness method,^[74] being exact in nature, is less sensitive to discretization errors, whereas the GDQ approach shows a modest error accumulation for higher frequencies. Despite these discrepancies, the agreement is within 6–8% for the most affected modes, which remains acceptable for engineering applications. More importantly, the fundamental and third modes show very close agreement (<2% error) with Banerjee's results,^[74] where the modes are more bending dominated. As the presence of other modes (such as twist) increase, the difference also increases (Table 4).

4.2. Effect of Rotational Spring Supports at the Boundaries

Tables 5–9 show the effect of variation in rotational spring supports on the first four mode of frequencies for bidirectional Al-Terfenol-D functionally graded twisted beams. The stiffness value of the rotational and translational spring is varied from 100000 to zero. The damping coefficient value is considered as zero, while the twisting angle is changed from $\phi = 40^\circ$ to $\phi = 0^\circ$. The transverse and axial power indices for Aluminium and Terfenol-D are taken as 0.1. The porosity index with uneven porosity distribution is considered as 0.1. For the stiffness value $K_{LT} = K_{RT} = K_L = K_R = 100000$, the clamped–clamped boundary condition is obtained. The simply supported boundary condition is obtained with the stiffness value of $K_{LT} = K_{RT} = 0$ and $K_L = K_R = 100000$. These tables highlight the sensitivity of modal characteristics to changes in boundary rotational stiffness, providing a comprehensive quantitative understanding. Overall, the tabulated results clearly demonstrate that a reduction in rotational stiffness progressively lowers the imaginary component across

Table 5. Imaginary component for varying rotational stiffness (transition from CC-SS state) considering $K_L = K_R = 100000 \text{ Nm}^{-1}$ and $C_L = C_R = C_{LT} = C_{RT} = 0 \text{ N-sm}^{-1}$, $\phi = 40^\circ$, $m = n = 0.1$ and $\alpha = 0.1$.

$K_{LT} = K_{RT}$	Mode 1	Mode 2	Mode 3	Mode 4
100000	137.2069	332.8384	571.4630	846.5506
10000	137.1703	332.7501	571.3113	846.3236
1000	136.8129	331.8881	569.8337	844.1165
100	133.8436	324.8296	557.9223	826.6218
10	119.6991	295.0957	513.5008	768.5754
0	90.5637	258.0876	474.4704	729.0701

Table 6. Imaginary component for varying rotational stiffness (transition from CC-SS state) considering $K_L = K_R = 100000 \text{ Nm}^{-1}$ and $C_L = C_R = C_{LT} = C_{RT} = 0 \text{ N-sm}^{-1}$, $\phi = 30^\circ$, $m = n = 0.1$ and $\alpha = 0.1$.

$K_{LT} = K_{RT}$	Mode 1	Mode 2	Mode 3	Mode 4
100000	117.7658	286.2028	493.3021	736.9825
10000	117.7338	286.1257	493.1678	736.7770
1000	117.4197	285.3694	491.8538	734.7703
100	114.7333	279.0018	480.9796	718.4782
10	101.5958	251.5156	439.5849	663.5371
0	74.3177	217.8268	403.9177	626.8009

all four modes, indicating a softening of the system response. This effect becomes more pronounced as the twist angle ϕ decreases from 30° to 0° , with the lowest values observed under free-rotational conditions ($K_{LT} = K_{RT} = 0$). These results corroborate with the following discussions, emphasizing the coupled influence of boundary flexibility and skew angle on the vibrational behavior of the system.

The variation in fundamental mode of frequency with different twist angle for different stiffness value of $K_{LT} = K_{RT}$ is shown in **Figure 2A**. The results show an intricate interplay of support stiffness values and the twist-induced variation, leading to a quantifiable variation trend of the fundamental frequency. As the twist angle progresses from 0° to 40° , the fundamental bending mode frequency experiences a modest decline across all stiffness levels, suggesting that the geometric coupling induced by the twist slightly softens the bending mode (i.e., varying the twist angle modifies the beam's bending natural frequency). On the other hand, increasing the equal spring stiffness ($K_{LT} = K_{RT}$) from 10^2 to 10^5 (log scale) significantly raises the bending frequency for any specified twist angle, indicating a shift from near-free to effectively clamped boundary conditions. The increase in frequency with stiffness diminishes at the highest K values, indicating a tendency to asymptotically approach the fully constrained (clamped) frequency. It is evident that at each stiffness level, the twisted beam exhibits a lower bending frequency compared to the untwisted scenario—indicative of a distinct structural interaction between twist and bending dynamics. The twist geometry fundamentally modifies the response of the bending mode to variations in boundary stiffness, as it incorporates bending-torsional coupling. From a control standpoint, these trends suggest that actively adjusting the support stiffness can effectively modulate the bending vibration frequency; the stiffer the adjustable support,

Table 7. Imaginary component for varying rotational stiffness (transition from CC-SS state) considering $K_L = K_R = 100000 \text{ Nm}^{-1}$ and $C_L = C_R = C_{LT} = C_{RT} = 0 \text{ N-sm}^{-1}$, $\phi = 20^\circ$, $m = n = 0.1$ and $\alpha = 0.1$.

$K_{LT} = K_{RT}$	Mode 1	Mode 2	Mode 3	Mode 4
100000	95.9283	234.9167	411.8930	629.6410
10000	95.9014	234.8507	411.7735	629.4512
1000	95.6362	234.2014	410.6008	627.5922
100	93.2945	228.5710	400.6396	612.1500
10	81.3579	203.4192	361.7430	559.0947
0	56.9586	173.5742	329.1600	524.2964

Table 8. Imaginary component for varying rotational stiffness (transition from CC-SS state) considering $K_L = K_R = 100000 \text{ Nm}^{-1}$ and $C_L = C_R = C_{LT} = C_{RT} = 0 \text{ N-sm}^{-1}$, $\phi = 10^\circ$, $m = n = 0.1$ and $\alpha = 0.1$.

$K_{LT} = K_{RT}$	Mode 1	Mode 2	Mode 3	Mode 4
100000	71.2215	183.4249	339.6938	543.3170
10000	71.1996	183.3669	339.5824	543.1340
1000	70.9821	182.7946	338.4852	541.3371
100	68.9994	177.6981	328.9591	526.1389
10	58.2471	153.9848	290.7520	472.9520
0	37.8286	125.4816	259.5880	438.4634

the higher the natural frequency. Nonetheless, the twist angle of the beam fundamentally affects the effectiveness of this control. Greater twist angles require meticulous attention to bending-torsional coupling in the control design, as twisting not only lowers the baseline frequency but also subtly alters the sensitivity of that frequency to variations in stiffness. Therefore, an active control strategy, such as employing adaptive end springs or magnetostrictive actuation, is needed to consider the interaction between twist and stiffness to attain accurate vibration suppression and frequency tuning.

4.3. Effect of Twisting Angle

The distortion that a structural component would experience when vibrating at its natural frequency is characterized by the mode shape. Natural frequencies and mode shapes therefore depict how the structure responds in a vibrating environment. For a qualitative evaluation of the structural component's dynamics, the mode shape characteristic is useful. In this regard, **Figure 2B** shows the effect of twist angle on the fundamental mode shape in $z - x$ plane for a cantilever bidirectionally functionally graded twisted beam. In the current investigation, we have limited our analysis to 40° for presenting numerical results based on practical considerations in engineering structures.

Figure 2C shows the effect of porosity index and twisting angle on the fundamental frequency of the bidirectional functionally graded aluminium-Terfenol-D beams. The fundamental mode frequency of Al-Terfenol-D twisted beams is observed to drop when the porosity index rises. This is due to porosity being one of the structural imperfections that decreases the stiffness of the beam. **Figure 3A** shows the effect of porosity on the dynamic

Table 9. Imaginary component for varying rotational stiffness (transition from CC-SS state) considering $K_L = K_R = 100000 \text{ Nm}^{-1}$ and $C_L = C_R = C_{LT} = C_{RT} = 0 \text{ N-sm}^{-1}$, $\phi = 0^\circ$, $m = n = 0.1$ and $\alpha = 0.1$.

$K_{LT} = K_{RT}$	Mode 1	Mode 2	Mode 3	Mode 4
100000	54.8245	157.1259	283.2981	508.7361
10000	54.8042	157.0696	283.1960	508.5540
1000	54.6020	156.5127	282.1832	506.7631
100	52.7253	151.4906	272.7667	491.5052
10	42.0277	127.5163	258.5605	437.6247
0	23.8351	101.1516	227.1102	402.7156

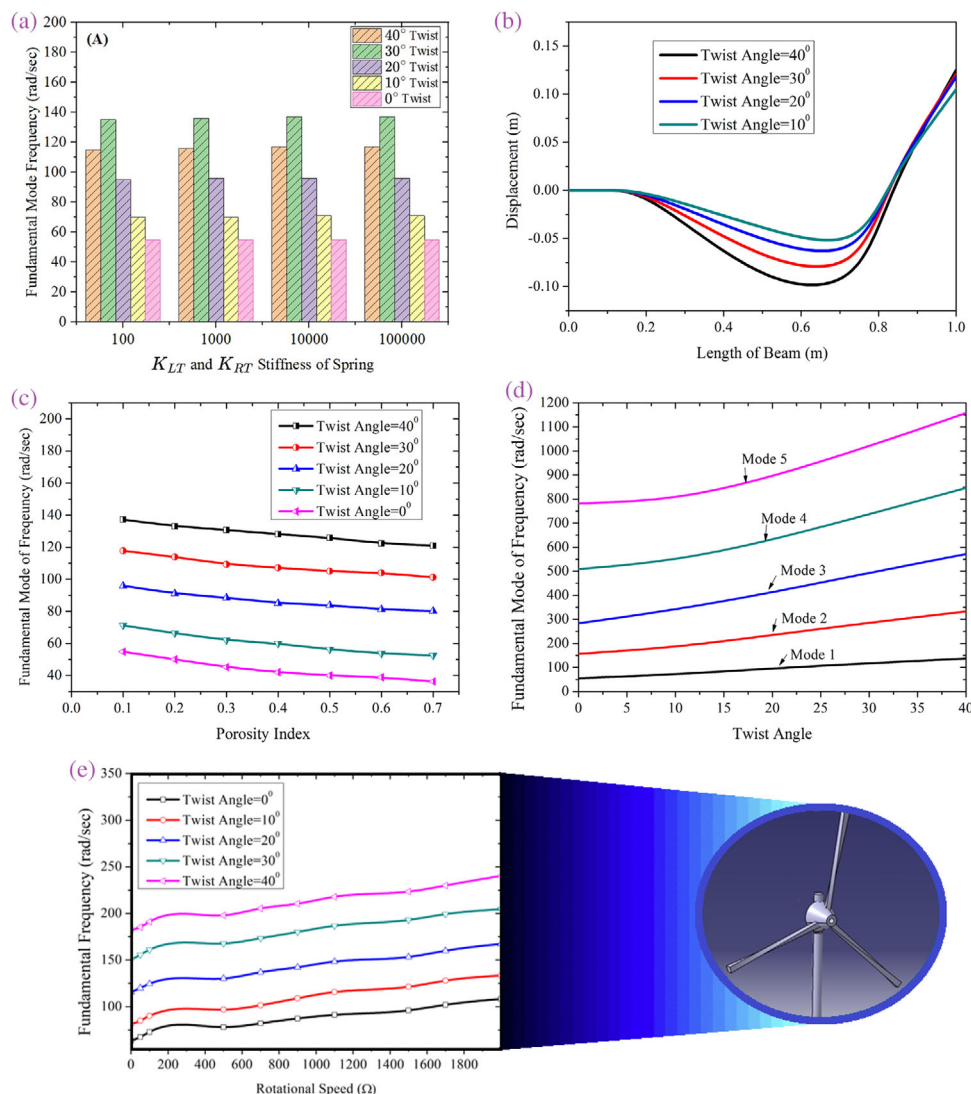


Figure 2. Twist-angle dependent dynamic behavior of bidirectional functionally graded aluminum-Terfenol-D beams. A) Variation of fundamental mode frequency with twist angle decay from clamped-clamped to simply supported boundary condition. B) Effect of twist angle on the fundamental mode shape of clamped-free bidirectional functionally graded Terfenol-D uneven porous beam. C) Effect of porosity index on fundamental mode frequencies of clamped-clamped bidirectional functionally graded Terfenol-D uneven porous beam. D) Effect of twist angle on clamped-clamped fundamental mode of bidirectional functionally graded Terfenol-D uneven porous beam. E) Rotational speed versus twisted beam frequency. The artistic visualization is provided for bringing context to the analysis, such as engineering application like turbines.

response of a twisted beam, wherein it becomes evident that the amplitude reduces with increased porosity. Figure 2D shows the variation of clamped-clamped natural frequencies of different modes with increasing twist angles. The effect of rotational speed on the lowest natural frequencies is shown in Figure 2E for the bidirectional functionally graded twisted beam. With the addition of centrifugal stiffening given by Equation (70) to the governing equation, the rotational effect is obtained for different twist angles. It is observed that, as the rotational speed Ω increases, the lowest natural frequency for the bidirectional functionally graded Al-Terfenol-D beam also increases. Figure 3B shows the effect of twist angle along with transverse and axial power indices on the natural frequencies of bidirectional functionally graded aluminium-Terfenol-D twisted beams. It is observed that the fun-

damental mode of frequency increases with an increase in twist angle as the transverse and axial power indices rise from 0 to 3.5.

The effect of twisting angle on the dynamic behavior of the Terfenol-D integrated twisted beams, as illustrated in Figures 2B–D and 3A–B, shows that increasing the twist angle redistributes the strain energy between bending and torsional modes, thereby altering the effective bending stiffness of the structure. This redistribution leads to strain energy localization at antinodes, which explains the frequency enhancement observed with higher twist angles. Simultaneously, the presence of porosity reduces the effective stiffness of the beam, counteracting the twist-induced stiffening and resulting in lower natural frequencies. The role of material gradation indices is also evident, as higher ceramic-rich gradation increases stiffness and

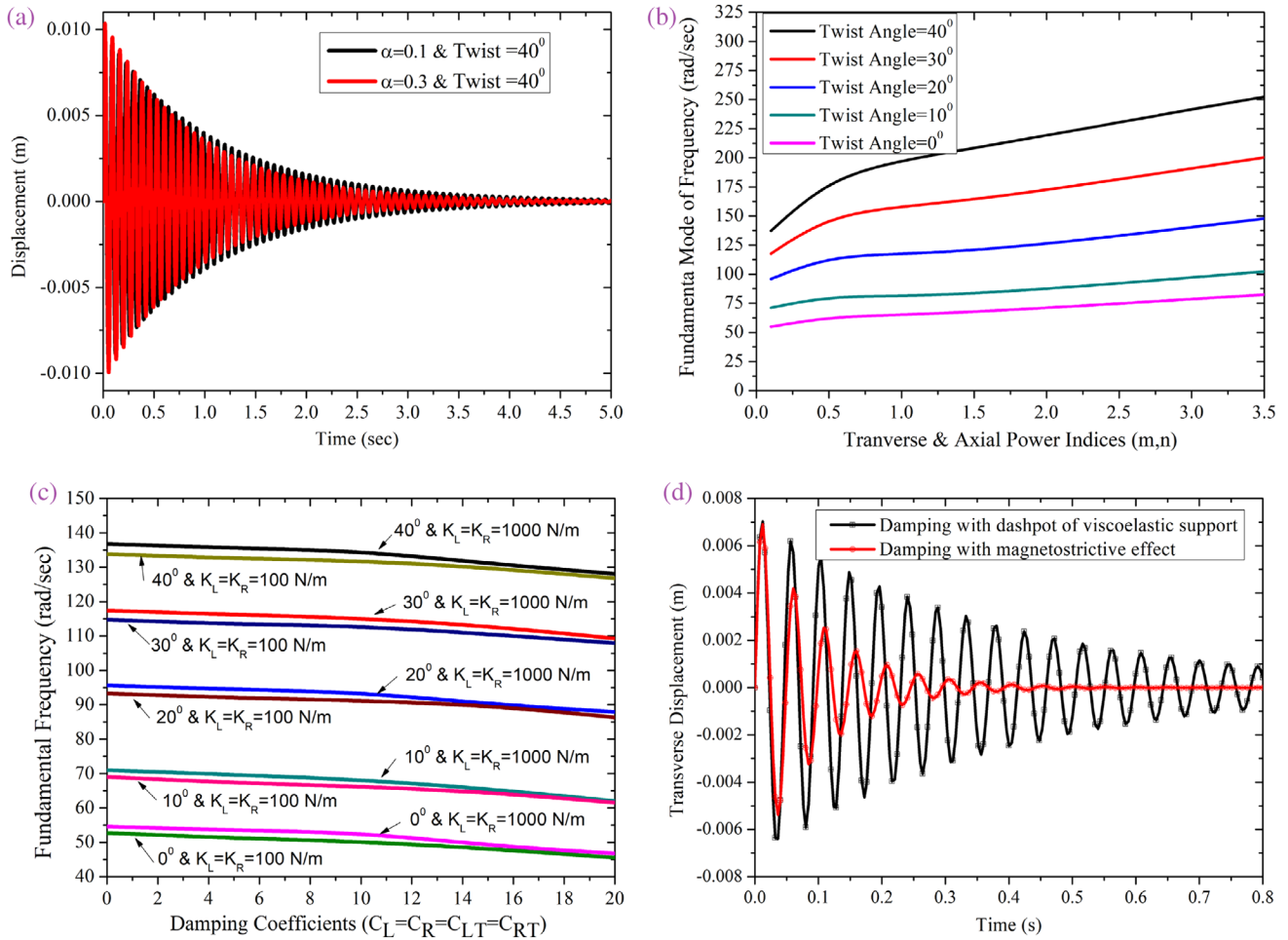


Figure 3. Effect of porosity, damping and gradation indices on the dynamic behavior. A) Effect of porosity index on dynamic response of simply supported bidirectional functionally graded Terfenol-D uneven porous beams. B) Effect of transverse and axial power indices on fundamental mode frequencies of clamped-clamped bidirectional functionally graded Terfenol-D uneven porous beams. C) Effect of damping dashpots on fundamental mode frequencies of bidirectional functionally graded Terfenol-D uneven porous beams (Parameters: $K_{LT} = K_{RT} = 10000$, $m = n = \alpha = 0.1$). D) Comparison of damping obtained with dashpots of viscoelastic support and with actuation of Terfenol-D on fundamental mode frequencies of bidirectional functionally graded Terfenol-D uneven porous beams (Parameters: $K_{LT} = K_{RT} = 10000$, $m = n = \alpha = 0.1$).

frequency, whereas metal-rich gradation promotes compliance and frequency reduction. Furthermore, the evolution of mode shapes with twisting (Figure 2B) can be physically interpreted as the reorientation of the principal stiffness axes: as the beam twists, bending and torsional responses couple more strongly, shifting the nodal patterns and amplifying stiffening effects in certain modes. Overall, these results highlight the interplay between twist-induced stiffening, porosity-driven softening, and gradation effects, offering a comprehensive explanation of the observed frequency trends.

4.4. Damping Effect Obtained Based on Dashpots and Terfenol-D

It's critical to investigate the damping effect contribution from the viscoelastic supports and Terfenol-D material. For a functionally graded beam made of bidirectionally varied aluminium and Terfenol-D concentrations, we explore and analyze the individual damping effect of dashpots and Terfenol-D. First, the com-

bined damping effect derived from modifications to the damping coefficients of viscoelastic supports and Terfenol-D material for uneven porous beams is shown in Figure 3C. The shift in the fundamental frequency of the twisted beam is observed to be minimal when the damping coefficients of viscoelastic end supports are increased from zero to 13 N sm^{-1} . However, when they surpass 13 N sm^{-1} , the frequency falls as the damping coefficient of the viscoelastic end supports increases for the different twist angles. The dampening effect for a bidirectional functionally graded aluminium-Terfenol-D twisted beam is shown in the Figure 3D with dashpots of viscoelastic support and Terfenol-D material actuation. Under the circumstances of free vibration, the beam's vibration is suppressed in 0.4 s, as shown by the red line, which is designed to illustrate the damping achieved with the magnetostrictive effect. Additionally, dampening achieved using dashpots of viscoelastic supports is illustrated using the black line. The dash-pot effect of viscoelastic supports has been shown to be less prominent than the magnetostrictive effect in terms of damping.

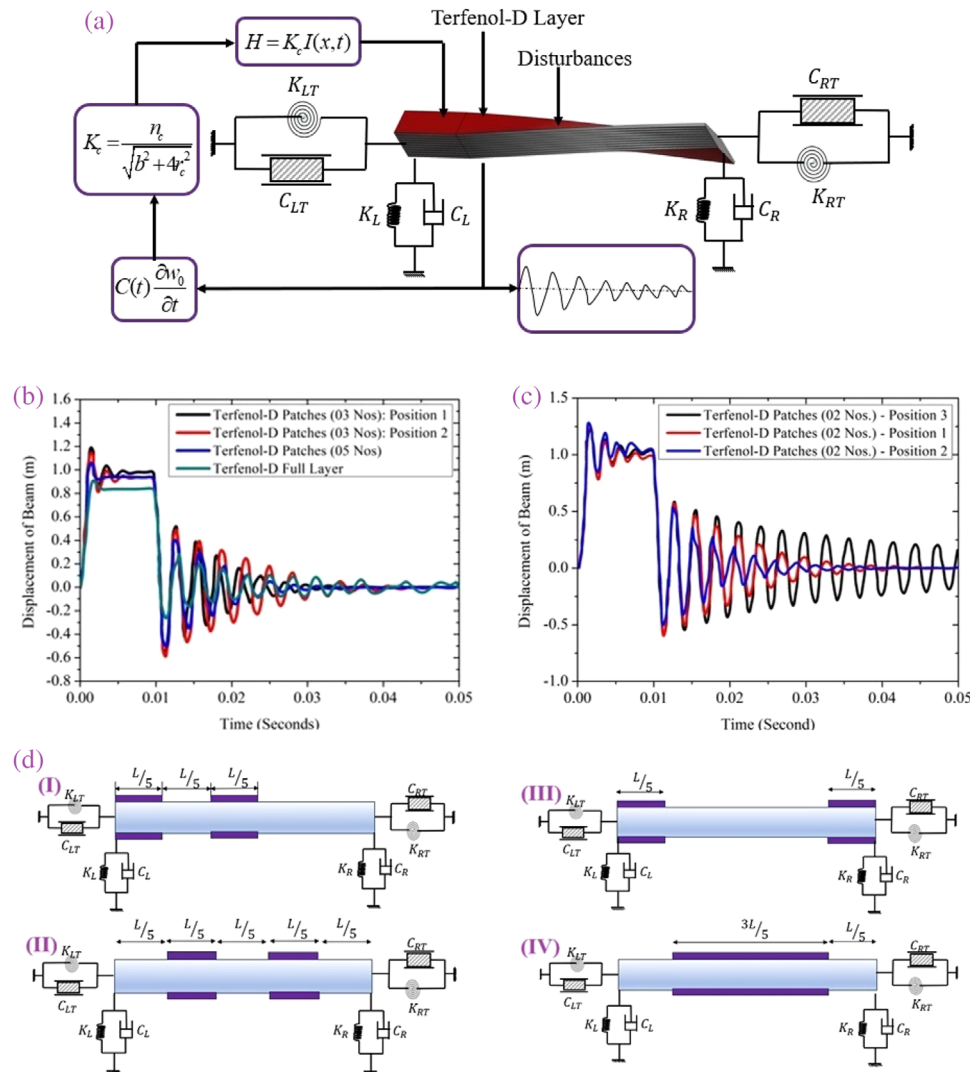


Figure 4. Vibration control of bidirectional functionally graded aluminum-Terfenol-D twisted beams. A) Control path with negative velocity feedback of viscoelastically supported twisted beams. B) Effect of different arrangement of three patches and full layer of Terfenol-D on the dynamics of twisted beams under transverse impulsive load. C) Effect of two Terfenol-D patches at different locations on twisted beam under transverse impulsive load. D) Representation of different configuration of bidirectional functionally graded aluminum-Terfenol-D twisted beams for dynamic control. I) Schematic illustration of two Terfenol-D patches on twisted beams, noted as “(02 Nos.) – Position 1.” II) Schematic illustration of two Terfenol-D patches on twisted beams, noted as “(02 Nos.) - Position 2”. III) Schematic illustration of two Terfenol-D patches on twisted beams, noted as “(02 Nos.) - Position 3”. IV) Schematic illustration of three Terfenol-D patches on twisted beams, noted as “(03 Nos.) - Position 1”. The configurations with Terfenol-D patches (05 Nos) containing five pairs of patches at $L/5$ distance apart and Terfenol-D full layer are not shown here as there are quite straightforward to visualize.

The viscoelastic dashpot dissipates energy primarily through passive viscous resistance, which is frequency- and temperature-dependent, leading to limited damping efficiency at higher vibration frequencies. In contrast, the magnetostrictive layer provides active magneto-mechanical coupling, where strain in Terfenol-D induces an opposing magnetic field-controlled stress that can be tuned almost instantaneously. This mechanism offers two advantages: i) Speed of response: Magnetostrictive actuation is governed by domain rotation in the material under applied bias field, enabling a near-instantaneous response to vibration cycles, unlike the slower relaxation times of viscoelastic media. ii) Magnitude and adaptivity of damping force: The induced magneto-mechanical stress adds to the structural stiffness and dissipative

effect, resulting in stronger suppression of vibration amplitude. Moreover, it can be actively tuned by adjusting the bias magnetic field, unlike the fixed damping coefficient of dashpots. Thus, the superior damping with magnetostrictive integration (as shown in Figure 3D) is attributed to faster dynamic response and higher controllable energy dissipation capacity compared to viscoelastic supports.

4.5. Control of Twisted Smart Beams

Figure 4A–C shows the control aspects of bidirectional functionally graded twisted beams. The schematic for the active vibra-

tion control strategy of the beams using negative velocity feedback control is shown in Figure 4A. The investigation focuses on evaluating the effectiveness of different pairs of patches placed in distinct configurations (refer to Figure 4D), along with complete Terfenol-D layers, as shown in the Figure 4B,C under the effect of transverse impulsive load. The application of impulsive loading first results in a rise and subsequent drop in the value of dynamic response. It is revealed through numerical experiments that the five Terfenol-D patches, positioned at a distance of $\frac{L}{5}$, is the most effective configuration for damping.

Parametric investigations are conducted here to demonstrate the impact of gain control and the characteristics and arrangement of Terfenol-D patches on the dynamic response of active sandwich beams under transverse impulsive loads. In general, the findings show that the implementation of active vibration control through exploiting the magnetostrictive qualities of Terfenol-D has a significant impact on reducing the oscillations of bidirectional functionally graded beams. Further, tailoring the material's responsiveness to external magnetic fields, as investigated in Figure 4, improves magnetostrictive control.

In this context, the evolving trends of architected matter and metastructures may be noted where placement of active elements and optimal material distribution play a key role.^[76–79] The improved damping performance of the five-patch configuration here is primarily due to enhanced spatial coverage of high-strain regions along the beam. Magnetostrictive patches are most effective when located near the strain antinodes of the fundamental bending mode, where curvature (and thus induced magneto-mechanical stress) is maximum. With fewer patches (e.g., 2 or 3), some high-strain regions remain underutilized, leading to less efficient energy extraction and control. By increasing to five patches, the coverage extends over multiple antinodes, ensuring that the induced counteracting stresses are more uniformly distributed and better synchronized with the modal deformation. Thus, the superiority of the five-patch layout arises from i) optimal alignment with modal strain distributions, ii) increased effective control authority through distributed actuation, and iii) reduction of localized untreated regions that can sustain vibration energy. This mechanism explains the trends in Figures 4B–C and underscores the importance of patch placement relative to mode shapes.

5. Concluding Remarks

In this study, free vibration analysis of bidirectional functionally graded aluminium-Terfenol-D beams with manufacturing flaws and twisted geometry is carried out under the influence of viscoelastic boundary conditions. Based on a first order shear deformation formulation, the governing differential equations of motion for the twisted beam are derived for free vibration. The computationally efficient differential quadrature technique is subsequently implemented to solve the resulting equations. The convergence and comparative assessments demonstrate that the developed computational model is accurate with respect to available literature. The differential quadrature approach is more precise and uses less computational resources than the dynamic stiffness and finite element method for investigating how structures evolve over time, particularly those with intricate forms or boundary conditions.

Pre-twisted beams are one of the most crucial structural components and are widely employed in several contemporary industrial sectors, including nuclear, automotive, aerospace, and renewable energy. One of the main causes of vibration is the dynamic forces imparted by the spinning cantilever beams. These structures must be operated safely and effectively, which requires vibration analysis and suppression. This paper has brought forth novel insights on the free vibration and smart control of complex structural geometries with twist.

Based on the developed computational model, the influences of twist angle, viscoelastic boundary condition, and the variation of transverse and axial power indices are investigated on the natural frequencies and mode shapes with the notion of developing a design-oriented mapping of the input parameter space. Two different types of porosity distribution patterns considering even and uneven porosity are analyzed to simulate the effect of manufacturing flaws. The fundamental mode frequency of the graded Al-Terfenol-D twisted beams is observed to drop when the porosity index rises. Additionally, the fundamental frequency changes as the twist angle increases. The shift in the fundamental frequency of the twisted beam is reported to be minimal when the damping coefficient of viscoelastic end supports is increased from 0 to 13 N sm⁻¹. As the rotational speed increases, the lowest natural frequency for the bidirectional functionally graded Al-Terfenol-D beam also increases. Further, computational investigations are conducted to demonstrate the impact of gain control, and the characteristics and arrangement of Terfenol-D patches on the dynamic response of active sandwich beams under transverse impulsive loads. The findings show that the implementation of an active vibration control technique through exploiting the magnetostrictive qualities of Terfenol-D can have a significant impact on reducing the oscillations of bidirectional functionally graded beams. In addition, tailoring the material's responsiveness to external magnetic fields through optimal placement of the Terfenol-D patches can improve magnetostrictive actuation, control, and sensing further. On the basis of this paper's results and insights, future study can be undertaken on non-linear vibration and dynamics of composite laminated blades with high rotation velocity.

Author Contributions

M.A.P. performed methodology, formulation, data generation, software, code development, and writing-original manuscript. T.M. performed supervision and reviewing manuscript. S.N. performed conceptualization, supervision, reviewing manuscript, and funding acquisition.

Conflict of Interest

The authors declare no conflict of interest.

Data Availability Statement

The data that support the findings of this study are available from the corresponding author upon reasonable request.

Keywords

bidirectional functionally graded beams, differential quadrature method, dynamics and control of Terfenol-D beams, gradation of Terfenol-D, viscoelastic supports

Received: July 16, 2025
Revised: September 10, 2025
Published online:

- [1] S.-C. Choi, J.-S. Park, J.-H. Kim, *J. Sound Vib.* **2007**, *300*, 176.
- [2] D. Vadiraja, A. Sahasrabudhe, *Thin Walled Struct.* **2009**, *47*, 555.
- [3] K. Singh, K. B. Shingare, T. Mukhopadhyay, S. Naskar, *Adv. Theory Simul.* **2023**, *6*, 2200756.
- [4] A. Chaurha, P. Malaji, T. Mukhopadhyay, *Eur. Phys. J. Spec. Top.* **2022**, *231*, 1403.
- [5] R. P. Khandelwal, A. Chakrabarti, P. Bhargava, *AIAA J.* **2014**, *52*, 1896.
- [6] M. Khorasani, A. Eyvazian, M. Karbon, A. Tounsi, L. Lampani, T. A. Sebaey, *Smart Struct. Syst.* **2020**, *26*, 331.
- [7] R. P. Khandelwal, A. Chakrabarti, P. Bhargava, *J. Intell. Mater. Syst. Struct.* **2013**, *24*, 1927.
- [8] P. Topdar, A. Chakraborti, A. Sheikh, *Comput. Meth. Appl. Mech. Eng.* **2004**, *193*, 4591.
- [9] P. Topdar, A. H. Sheikh, N. Dhang, *AIAA J.* **2006**, *44*, 2636.
- [10] M. Selvan T, S. Sharma, S. Naskar, S. Mondal, M. Kaushal, T. Mondal, *ACS Appl. Mater. Interfaces* **2022**, *14*, 45921.
- [11] A. Khurana, S. Naskar, M. Joglekar, T. Mukhopadhyay, *Int. J. Eng. Sci.* **2024**, *196*, 103974.
- [12] S. Mondal, T. Mukhopadhyay, S. Naskar, *AIAA J.* **2025**, *63*, 1.
- [13] K. Shingare, S. Mondal, T. Mukhopadhyay, *Mech. Syst. Signal Process.* **2022**, *169*, 108757.
- [14] A. Khurana, S. Naskar, R. Varma, T. Mukhopadhyay, *Int. J. Eng. Sci.* **2024**, *194*, 103974.
- [15] D. Kundu, S. Naskar, T. Mukhopadhyay, *Philos. Trans. A* **2024**, *382*, 20230360.
- [16] A. Singh, T. Mukhopadhyay, S. Adhikari, B. Bhattacharya, *Smart Mater. Struct.* **2022**, *31*, 125005.
- [17] P. Sinha, T. Mukhopadhyay, *Smart Mater. Struct.* **2023**, *32*, 055021.
- [18] A. Singh, T. Mukhopadhyay, S. Adhikari, B. Bhattacharya, *Compos. Struct.* **2022**, *280*, 114857.
- [19] A. Singh, T. Mukhopadhyay, B. Bhattacharya, *Int. J. Solids Struct.* **2021**, *208*, 31.
- [20] D. Jha, T. Kant, R. Singh, *Compos. Struct.* **2013**, *96*, 833.
- [21] D. Punera, T. Kant, *Compos. Struct.* **2019**, *210*, 787.
- [22] T. Mukhopadhyay, P. Karsh, B. Basu, S. Dey, *Compos. Struct.* **2020**, *237*, 111870.
- [23] S. Naskar, T. Mukhopadhyay, S. Sriramula, *Compos. Struct.* **2019**, *209*, 940.
- [24] S. Dey, T. Mukhopadhyay, S. Adhikari, *Acta Mech.* **2015**, *226*, 2537.
- [25] A. Garg, H. Chalak, L. Li, M.-O. Belarbi, R. Sahoo, T. Mukhopadhyay, *Acta Mech. Solida Sin.* **2022**, *35*, 1.
- [26] P. S. Ghatage, V. R. Kar, P. E. Sudhagar, *Compos. Struct.* **2020**, *236*, 111837.
- [27] S. Dey, T. Mukhopadhyay, S. Sahu, S. Adhikari, *Eur. J. Mech. A. Solids* **2018**, *67*, 108.
- [28] K. Kalita, T. Mukhopadhyay, P. Dey, S. Haldar, *Neural Comput. Appl.* **2020**, *32*, 7969.
- [29] S. Dey, T. Mukhopadhyay, H. H. Khodaparast, S. Adhikari, *Period. Polytechnica Civil Eng.* **2016**, *60*, 103.
- [30] T. Mukhopadhyay, T. K. Dey, S. Dey, A. Chakrabarti, *Struct. Eng. Int.* **2015**, *25*, 173.
- [31] Vaishali, T. Mukhopadhyay, R. Kumar, S. Dey, *Compos. Struct.* **2021**, *262*, 113294.
- [32] A. Garg, S. Naskar, T. Mukhopadhyay, *Eng Comput* **2025**, *41*, 2291.
- [33] H. Deng, W. Cheng, *Compos. Struct.* **2016**, *141*, 253.
- [34] T. Van Do, D. K. Nguyen, N. D. Duc, D. H. Doan, T. Q. Bui, *Thin Walled Struct.* **2017**, *119*, 687.
- [35] A. Singh, S. Naskar, P. Kumari, T. Mukhopadhyay, *Mech. Syst. Signal Process.* **2023**, *184*, 109636.
- [36] S. Ghuku, S. Sahoo, T. Mukhopadhyay, *Int. J. Non Linear Mech.* **2025**, *168*, 104935.
- [37] P. Tiwari, S. Naskar, T. Mukhopadhyay, *Thin Walled Struct.* **2025**, *210*, 112901.
- [38] B. Lin, B. Chen, B. Zhu, J.-a. Li, Y. Li, *Thin Walled Struct.* **2021**, *164*, 107902.
- [39] C. Li, H. Cheng, *J. Sound Vib.* **2021**, *492*, 115791.
- [40] S. Dey, T. Mukhopadhyay, H. H. Khodaparast, S. Adhikari, *Compos. Struct.* **2015**, *131*, 594.
- [41] T. Y. Zhao, Y. Ma, H. Y. Zhang, H. G. Pan, Y. Cai, *Appl. Math. Modell.* **2021**, *93*, 578.
- [42] T. Y. Zhao, L. P. Jiang, H. G. Pan, J. Yang, S. Kitipornchai, *Compos. Struct.* **2021**, *262*, 113362.
- [43] H. Cheng, C.-f. Li, Y. Jiang, *Mech. Adv. Mater. Struct.* **2022**, *29*, 2040.
- [44] H. Guo, X. Ouyang, K. K. Žur, X. Wu, T. Yang, A. J. Ferreira, *Compos. Struct.* **2022**, *282*, 115129.
- [45] S. Lotfan, B. Bediz, *J. Sound Vib.* **2022**, *535*, 117109.
- [46] M. A. Patil, R. Kadoli, *Appl. Math. Modell.* **2020**, *84*, 137.
- [47] I. Bensaid, A. Saimi, *Aust. J. Mech. Eng.* **2023**, *21*, 1440.
- [48] W. Zhong, F. Gao, Y. Ren, *Math. Probl. Eng.* **2019**, *2019*, 1538329.
- [49] A. G. Shenas, P. Malekzadeh, S. Ziaee, *Compos. Struct.* **2017**, *162*, 325.
- [50] D. Adair, M. Jaeger, *Math Mech Solids* **2018**, *23*, 1345.
- [51] X. Wang, Z. Yuan, *Comput. Math. Appl.* **2018**, *76*, 1486.
- [52] V. Ondra, B. Titurus, *J. Sound Vib.* **2019**, *461*, 114912.
- [53] J. Wu, B. Titurus, *J. Sound Vib.* **2021**, *498*, 115980.
- [54] D. K. Nayak, M. Pradhan, P. K. Jena, P. Dash, *Noise Vibr. Worldwide* **2021**, *52*, 385.
- [55] T. D. Singha, T. Bandyopadhyay, A. Karmakar, *Mech. Adv. Mater. Struct.* **2023**, *30*, 3013.
- [56] Y. Chen, T. Ye, G. Jin, S. Zhong, W. Lv, Q. Mao, *Mech. Syst. Signal Process.* **2025**, *222*, 111721.
- [57] H. Zhang, C. Li, T. Jia, *Mech. Based Des. Struct. Mach.* **2024**, *52*, 4667.
- [58] W. Zhang, X. Gu, Y. Zhang, *Thin Walled Struct.* **2023**, *184*, 110523.
- [59] X. Gu, W. Zhang, Y. Zhang, *Compos. Struct.* **2023**, *315*, 116936.
- [60] M. Yao, S. Wang, Y. Niu, Q. Wu, C. Wang, *Appl. Math. Modell.* **2024**, *128*, 392.
- [61] S. Bhattacharya, D. Das, *Proc. Inst. Mech. Eng. Part L J. Mater. Des. Appl.* **2020**, *234*, 21.
- [62] S. K. Shada, S. Kattimani, R. MR, *Mech. Adv. Mater. Struct.* **2024**, *31*, 1.
- [63] V. M. Kuriakose, V. Sreehari, *Compos. Part C: Open Access* **2023**, *11*, 100361.
- [64] M. A. Patil, R. Kadoli, *J. Braz. Soc. Mech. Sci. Eng.* **2020**, *42*, 591.
- [65] M. A. Patil, R. Kadoli, *J. Braz. Soc. Mech. Sci. Eng.* **2023**, *45*, 357.
- [66] M. A. Patil, R. Kadoli, S. Saraf, S. Naskar, *Mech. Based Des. Struct. Mach.* **2024**, *52*, 7138.
- [67] M. A. Patil, R. Kadoli, *Mech. Adv. Mater. Struct.* **2023**, *30*, 4685.
- [68] M. A. Patil, R. Kadoli, *Eng. Res. Express* **2024**, *6*, 035553.
- [69] M. A. Patil, S. Saraf, R. Kadoli, S. Naskar, *Mech. Based Des. Struct. Mach.* **2024**, *52*, 1.

- [70] A. Oudra, Y. E. Khouddar, A. Adri, O. Outassafte, I. E. Hantati, H. Isksiou, H. E. Moussami, *ZAMM-J. Appl. Math. Mech./Zeitschr. Angew. Math. Mech.* **2024**, *104*, e202400236.
- [71] H. Bellifa, M. M. Selim, A. Chikh, A. A. Bousahla, F. Bourada, A. Tounsi, K. H. Benrahou, M. M. Al-Zahrani, A. Tounsi, *Smart Struct Syst* **2021**, *27*, 719.
- [72] O. Taleb, M. Sekkal, R. Bachir Bouiadjra, S. Benyoucef, A. Tounsi, M. M. Selim, K. M. Khedher, *Mech. Based Des. Struct. Mach.* **2024**, *53*, 1045.
- [73] J. Reddy, J. Barbosa, *Smart Mater. Struct.* **2000**, *9*, 49.
- [74] J. Banerjee, *Int. J. Solids Struct.* **2001**, *38*, 6703.
- [75] S. Pradhan, T. Murmu, *J. Sound Vib.* **2009**, *321*, 342.
- [76] S. Mondal, T. Mukhopadhyay, S. Naskar, Active heterogeneous mode coupling in bi-level multi-physically architected metamaterials for temporal, *Commun. Eng.* **2025**, *4*, 103.
- [77] P. Tiwari, S. Naskar, T. Mukhopadhyay, *AIAA J.* **2023**, *61*, 1820.
- [78] D. Kundu, S. Ghuku, S. Naskar, T. Mukhopadhyay, *Adv. Eng. Mater.* **2023**, *25*, 2201407.
- [79] R.-H. Fan, B. Xiong, R.-W. Peng, M. Wang, *Adv. Mater.* **2020**, *32*, 1904646.